Clockwork Orangutan: microRNAs, thermoregulatory tradeoffs, and the evolution of brain size.

Bastian Fromm*, PhD
The Arctic University Museum of Norway
UiT- The Arctic University of Norway 9037
Tromsø, Norway

Thomas Sorger, PhD
Department of Biology
Roger Williams University
Bristol, Rhode Island 02809, USA

* corresponding author

ABSTRACT

Homeostasis of body temperature (T_b) requires that internal heat generation associated with evolutionary increases in brain size must have been matched by more rapid heat dissipation and/or a reduction in thermogenesis by other organs ('expensive tissue hypothesis') [1-2]. Since the rate of liver gluconeogenesis during human development varies inversely with the rate of body growth [3-6], we postulated a phylogenetic tradeoff between liver thermogenesis and that of other organs, governed by body size. We found that relative to a thermogenic Core (kidney, heart, liver and brain), the mass-independent residuals of liver and brain were strictly anti-correlated, as were their cellular metabolic rates (*cMR*s), estimated by regression on body size and the number of microRNA families (*mirFam*) [7]. A linear model of Core thermogenesis exhibited a joint *cMR* that scaled allometrically as $M^{0.53}$, consistent with a comprehensive biophysical model of thermoregulation [8]. A positive feedback relationship between brain size and *mirFam*, a proxy for energy reliability, fit a logistic function. In conjunction with variable rate phenograms, this model detected size adaptation to a low-energy regime among the smallest primates and, among primates with the largest brains, thermoregulatory adaptation to the limit on the rate of heat dissipation.

INTRODUCTION

The diversification of mammalian orders has been characterized by two long-term trends: increasing size [9] and decreasing body temperature [10]. Resting metabolic rate (*rMR*), in contrast, has not exhibited a long-term trend, but, in coordination with variation in thermal conductance (C_{min}), has allowed mammals across the entire range of size to occupy nearly the entire range of climatic zones [10-12], albeit with a narrower range of tolerance to heat than to cold [13-15]. These trends are explicable by a physiological limit on the rate of heat dissipation, initially proposed by Speakman and Król (2010) [16]. Notwithstanding this evidence, current models to account for increasing brain size in the human lineage do not consider thermoregulatory constraints [17-18].

The human brain's power consumption of 15W raises the temperature of its venous outflow by ~ 0.2 - 0.3ºC [19-22]. Orangutans are similar to humans in body size, but their brains are ⅔ smaller and generate heat at a rate of only 4W [23]. Given that ~ 15% of human blood volume perfuses the brain every minute [24], this suggests a significant thermoregulatory challenge that can be addressed in only two ways: a faster rate of heat dissipation or a tradeoff in energy expenditure with another metabolically expensive tissue, such as kidney, heart, liver or intestine [1-2]. Like chimpanzees [25], ancestral humans most likely relied on behavioral thermoregulation to avoid hyperthermia in hot environments which, however, did not address the problem of internal heat generation. Adaptations

for heat dissipation that are unique to humans include hairlessness, bipedalism, and a 10-fold increase in the density of eccrine sweat glands relative to densities found in chimpanzees and macaques [26], an adaptation that may have also increased the risk of dehydration [27].

Despite numerous attempts, the effort to detect tradeoffs predicted by the 'expensive tissue hypothesis' has been abandoned since the publication of a study encompassing eight organs in 100 species, including 23 primates, that found no significant anticorrelations among the residuals for the log of organ mass regressed against body mass [28]. Rather than whole body mass, we postulated that the relevant standard for variation of the four most thermogenic organs (kidney, heart, liver and brain) is a composite Core fitting the comprehensive model of thermoregulation of Porter and Kearney (2009) [8]. We found that evolutionary increases in the proportion of the brain in this Core were offset by decreases in the proportion of the liver, with a corresponding anticorrelation between their Core mass-independent residuals.

We have previously demonstrated that, unlike log-based specific *MR*s (*sMR*s), *mirFam*-based cellular *MR*s (*cMR*s) are robust to variation in the range of mass and sensitive to body temperature [7]. In the present study, we estimated the cellular *MR* (*cMR*) of each Core organ based on criteria:

a) correlation with organ size and *mirFam* (physiological relevance) [7];
b) correspondence between the joint *cMR* of these organs and the predicted rate of core thermogenesis ($\propto \sqrt{M}$) [8] (thermodynamic relevance);
c) utility for the unsupervised classification of major primate clades (phylogenetic relevance).

We found that liver *cMR*s were anticorrelated with body mass and with the *cMR*s of kidney, heart and brain. The joint *cMR* of this 4-organ Core ($M^{0.53}$) scaled close to the theoretical rate of thermogenesis, unlike the joint *sMR* derived from the log-based *sMR* of each organ. Since the liver is the primary organ of gluconeogenesis in fasting or starvation, the liver-brain anticorrelations are consistent with an energy-limited, positive feedback model of brain size evolution [17-18].

RESULTS

The proportion of brain mass in the Core varies reciprocally with that of liver

Of the six possible tradeoffs in a Core consisting of four thermogenic organs, one major tradeoff occurred consistently among primate clades, that between brain and liver (Figure 1A, B). A dampened tradeoff between heart and kidney occurred approximately "in phase" with the major tradeoff. Brain and liver proportions in the Core also varied reciprocally across 30 additional Euarchontoglires, with a diminished tradeoff between heart and kidney (Supplementary Figure S1).

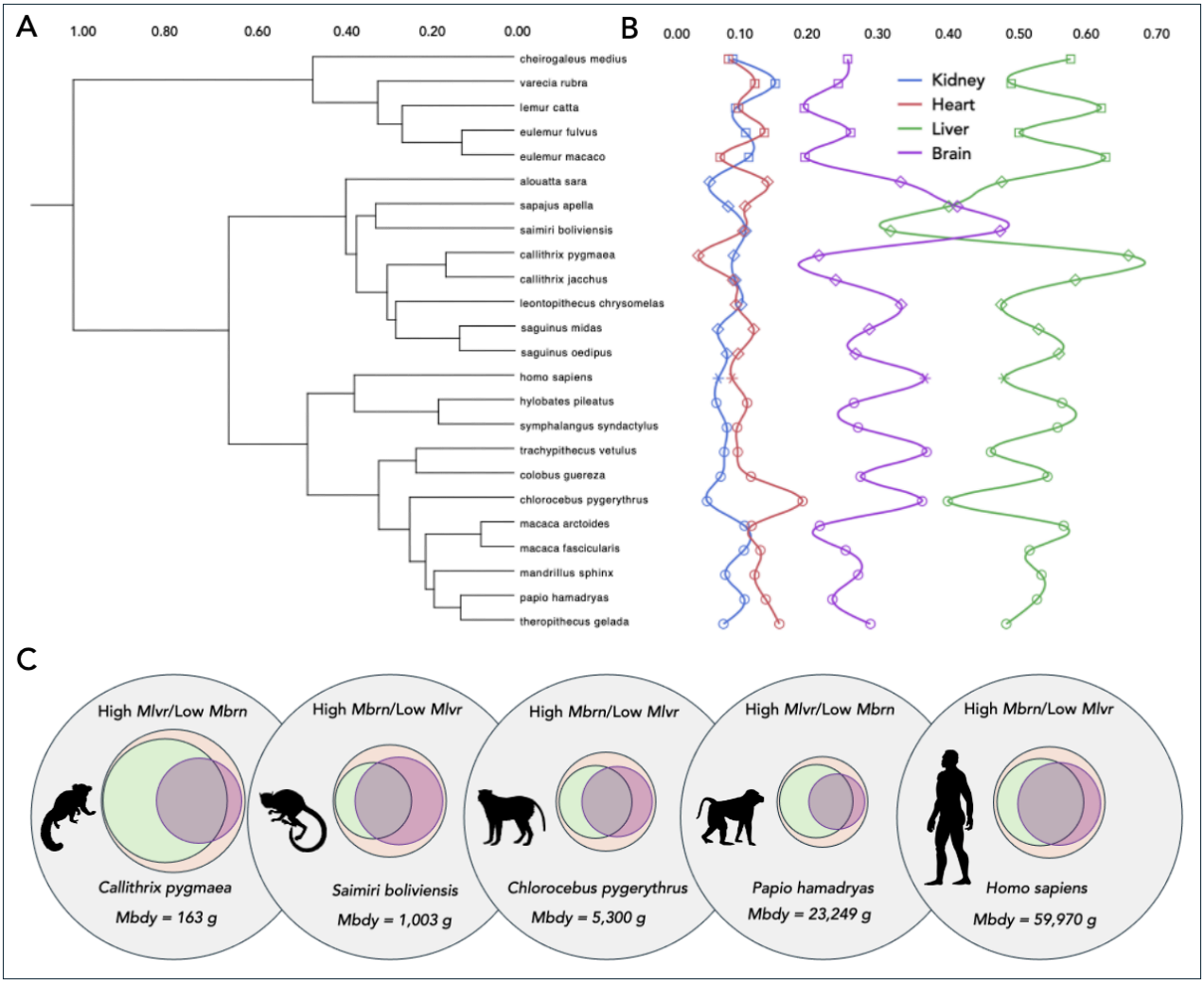

Figure 1. The proportion of brain mass in the Core varies reciprocally with that of the liver.
A. Time tree of 24 primates (scale bar represents the relative time of divergence).
B. Mass proportion of each organ relative to the total Core mass.
C. Summary model comparing representative species with low or high ratios of brain/liver mass. The radius of each circle represents a spherical volume corresponding to relative organ or Core mass. The relative proportions of liver and brain are represented by green and purple circles, respectively. Silhouttes: *Callithrix jacchus*, *Saimiri* (generic), *Erythrocebus patas*, *Papio* (generic), *Homo sapiens idaltu* (© Phylopic 2024, compiled by T. Michael Keesey).

Tradeoffs between liver and brain masses were readily demonstrable with log-transformed data, provided that they were ranked according to Core size (Figure 2C) rather than body size (Figure 2A). Residuals of the regressions exhibited a periodic pattern of variation for each organ, corresponding to the relative proportion of body mass (Figure 2B) or Core mass (Figure 2D). Since the tradeoff between the residuals of brain and liver mass is apparent only when ranked according to Core mass (Figure 2D versus Figure 2B), standardization of log *Mbrn* with respect to log *Mbdy* precludes its detection [28].

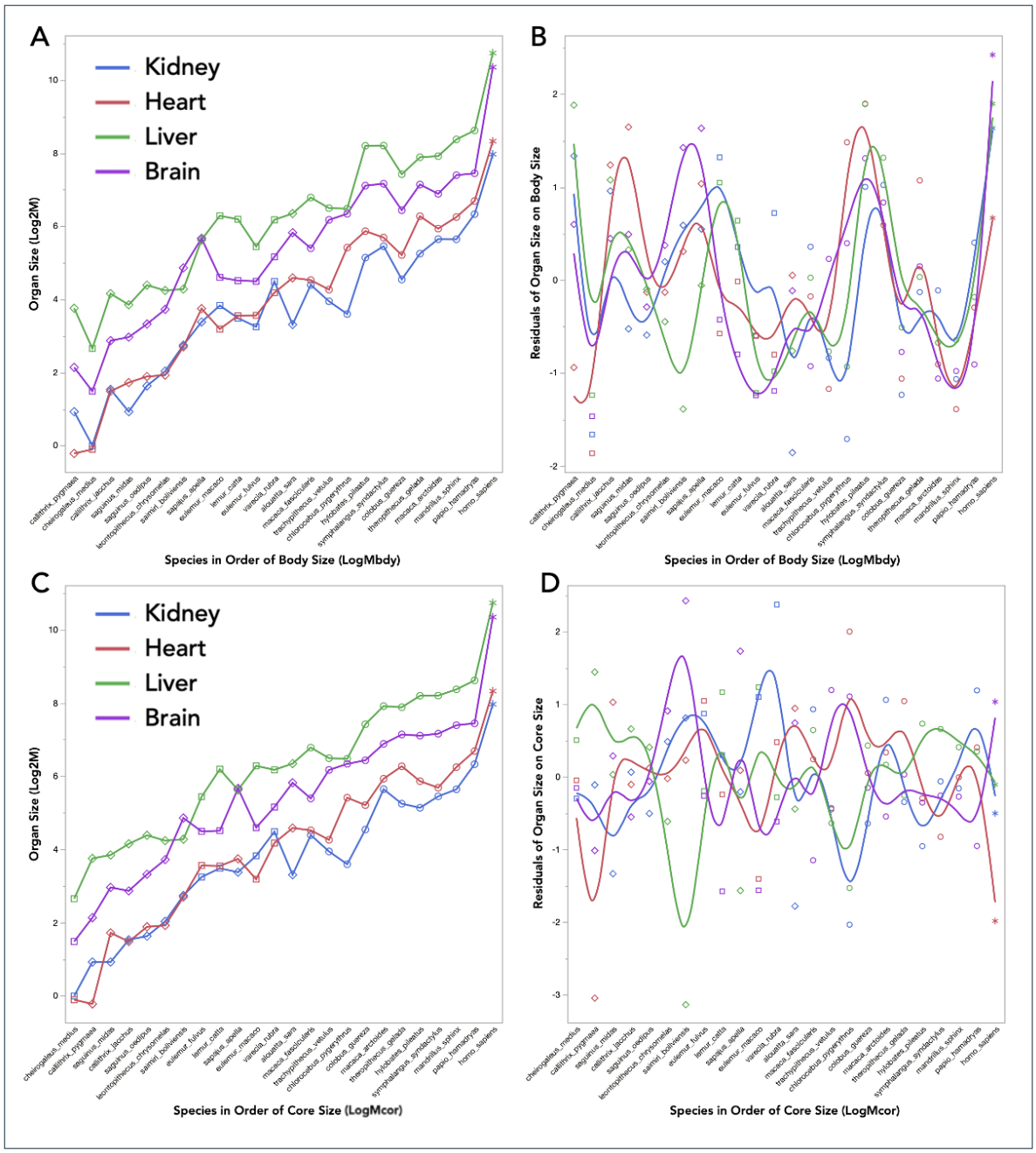

Figure 2. The reciprocal variation between liver and brain mass in the Core.
A and C: Variation of organ size relative to body size and Core size in primates.
B and D: Mass-independent residual variation relative to body size and Core size in primates.

Physiologically-based cMRs do not correspond to log-based sMRs

Assuming power law models, we distinguish between:

specific *MR* (*sMR*): $sMR = m \times M^b$,

where b is the slope of log *rMR*/log *M*, and

cellular *MR* (*cMR*): $cMR = n \times M^c$,

where c is the allometric exponent obtained by maximum likelihood fitting of rMR/M^c to the distribution of a physiologically-relevant trait, such as *mirFam* [7]. A log-based *sMR* has a fixed value across a set of species, regardless of size, and therefore the ratio of *sMR* to a non-logarithmic trait is uninformative (Supplemental Figure 2A). A *mirFam*-based *cMR* increases or decreases as a function of size (Supplementary Figure 2B), yielding a biologically informative rank order for *cMR*/trait ratios (Supplementary Figure S3), with implications for phylogenetic covariance models [29, 32-35].

Estimation and physiological relevance of thermogenic organ cMRs

We previously demonstrated that variable allometric scaling, in conjunction with phylogenetic regression, yielded $M^{0.71}$ as the optimal scaling of *cMRbdy* (hence *cMR.71bdy*) with respect to *mirFam* across 10 representative mammals [7]. In order to estimate *mirFam*-based *cMR*s for each of the four thermogenic organs, we compared the dependence of *cMR* in the range *cMR.60* - *cMR.90* on both *mirFam* and organ mass, revealing two distinct patterns of slope inversion: one for kidney, heart and brain (inversions at $\geq M^{0.80}$), another for the liver and whole body (inversions at $M^{0.70}$) (Figure 3).

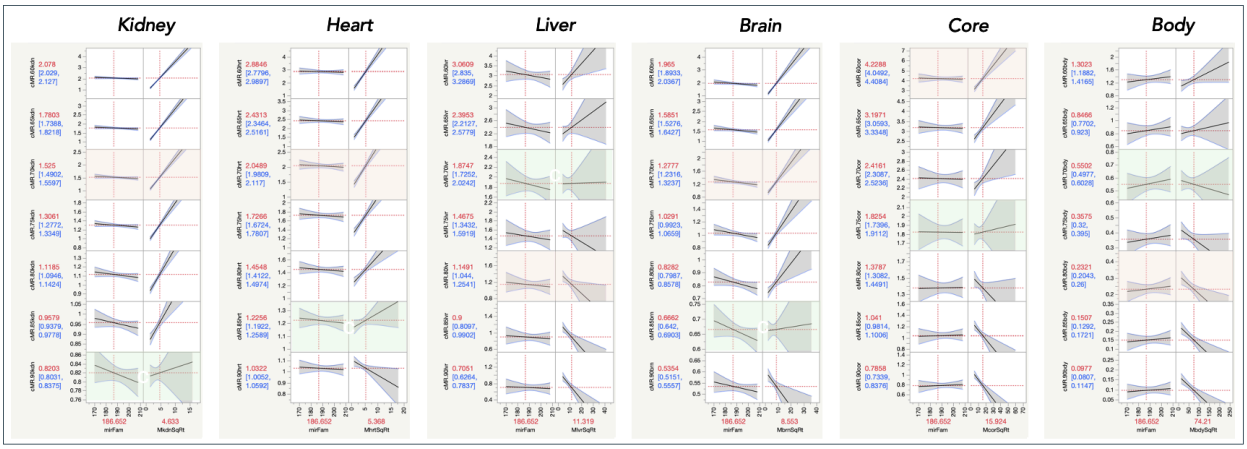

Figure 3. Dependence of *cMR* on $\sqrt{Morg}$ and *mirFam* in 22 primates.
$\sqrt{M}$, a natural scale for *cMR*s, yielded *P* values several orders of magnitude lower than did a log scale. Estimated *cMR* slopes are shaded pink, whereas log-based *sMR* slopes are shaded green. Note that the log-based *sMR*s correspond to crossover points for the inversions of the *cMR* slopes. Values in red represent means (± CI).

Assuming an operating range of $M^{0.70}$ - $M^{0.80}$, we estimated each organ's *cMR* based on the lowest *P* value of the multiple regressions, hence *cMR.**70**kdn*, *cMR.**70**hrt*, *cMR.**70**brn* and *cMR.**80**lvr*. For each organ, the log-based *sMR* corresponded to the crossover point for the inversion of the *cMR* slopes, *i.e.* the zone of minimal correlation with *mirFam* and body size, and therefore also of minimal constraint by these factors (Figure 3). The Core alone exhibited an *sMR* with the Kleiber exponent ~ 0.75 (0.756), which was previously shown to be the optimal scaling of *cMRbdy* with respect to *mirFam* in a model of stabilizing selection across 10 representative mammals [7].

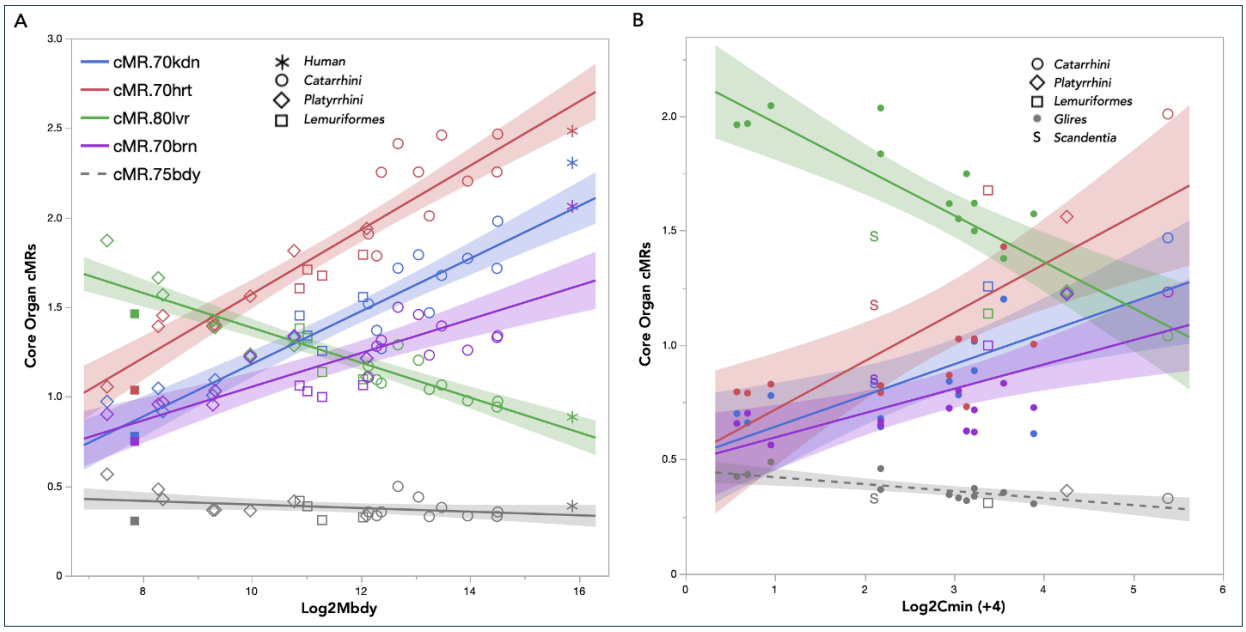

Figure 4. Core organ *cMR*s as a function of body size or thermal conductance.
A. Primates ($N = 24$). Filled symbols represent a heterotherm.
B. Euarchontoglires ($N = 16$). Shaded bands: confidence interval for each regression.

Plotting these *cMR*s as a function of primate whole body size revealed a strong anticorrelation between liver *cMR.80* and the *cMR.70*s of the other organs that established an overall negative slope of *cMR.75bdy* with respect to *Mbdy* (Figure 4A). Similar slopes were obtained when plotting organ *cMR*s against the minimal thermal conductance (C_{min}) of 16 Euarchontoglires (Figure 4B), pointing to a common origin for these physiological and thermoregulatory relationships. C_{min} is an extensive property that depends primarily on total surface area and secondarily, on the properties of the insulating layer [36]. Like organ size, it is expected to increase geometrically with body size [8]. Ranking primates according to log C_{min} revealed a tradeoff in *cMR*, but not a mass, between liver and the other Core organs (Supplementary Figure S4).

We tested the relevance of these estimated core organ *cMR*s against thermodynamic and phylogenetic models. For a steady state (whole animal) resting *MR* that scales as $M^{0.75}$, the rate of Core thermogenesis has been predicted to scale approximately as √M ($M^{0.50}$) [8]. We applied partial least squares regression [37] in order to predict the optimal scaling of a joint Core *cMR* composed of either *mirFam*-based *cMR*s or the log-based *sMR*s for the four thermogenic organs, hence:

$$cMR.Xcor = (rMRkdn + rMRhrt + rMRlvr + rMRbrn) / (Mkdn + Mhrt + Mlvr + Mbrn)^X$$

$$= (a \bullet cMR.\mathbf{70kdn}) + (b \bullet cMR.\mathbf{70hrt}) + (c \bullet cMR.\mathbf{80lvr}) + (d \bullet cMR.\mathbf{70brn})$$

OR

$$sMR.Xcor = (rMRkdn + rMRhrt + rMRlvr + rMRbrn) / (Mkdn + Mhrt + Mlvr + Mbrn)^{X}$$

$$= (a' \bullet sMR.\mathbf{90kdn}) + (b' \bullet sMR.\mathbf{87hrt}) + (c' \bullet sMR.\mathbf{67lvr}) + (d' \bullet sMR.\mathbf{83brn})$$

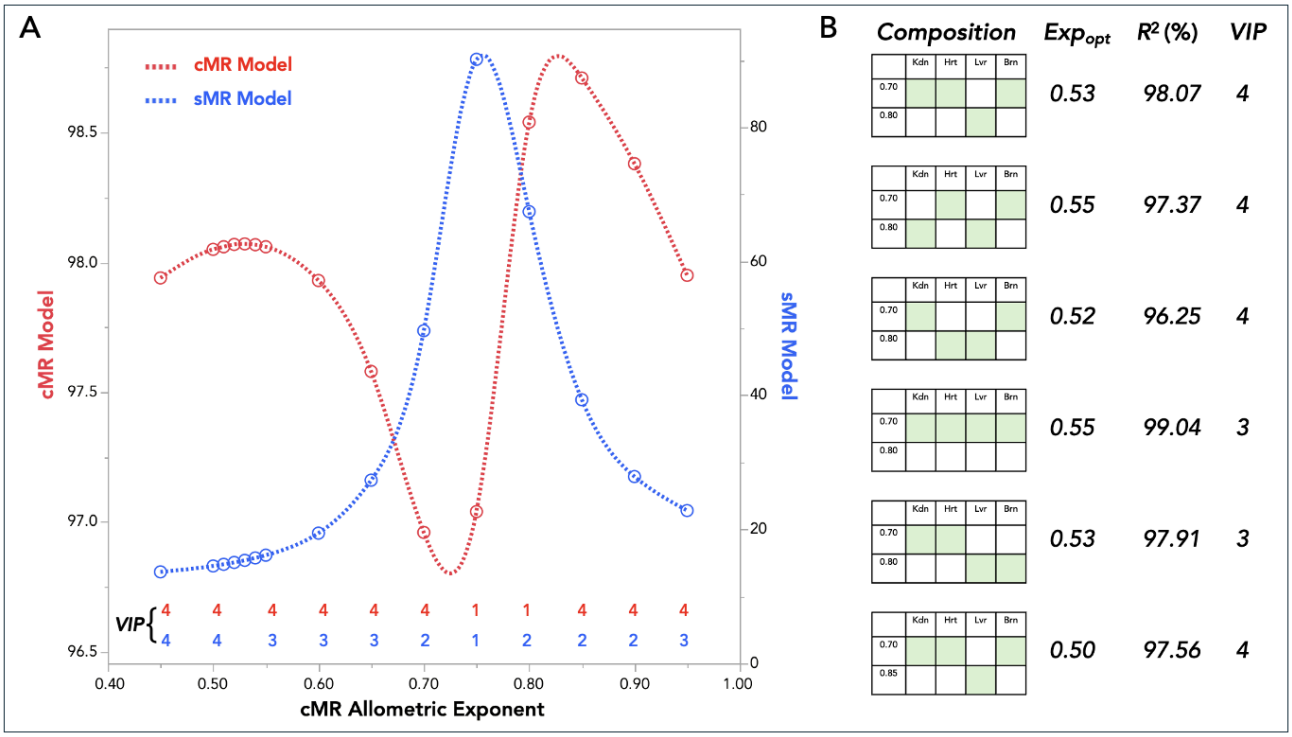

Figure 5. R^2 (% variation) for models of *cMRcor* predicted by linear combinations of *mirFam*-based *cMR*s or log-based *sMR*s of the four thermogenic organs (note the difference in scales; $N = 22$).
A. Comparison between *mirFam*-based organ *cMR*s and log-based organ *sMR*s. Below the plot the table of values for *VIP* (*variable importance of projection*) indicates the number of organs upon which each the model is significantly dependent.
B. Comparison of combinations of *cMR.70* and *cMR.80* among the four thermogenic organs.
Exp_{opt}: the optimally fitting Core allometric exponent for the linear model.

The *cMR* model exhibited a broad peak centered at $M^{0.53}$, similar to that predicted by the biophysical model of core thermogenesis [8], and a second peak between $M^{0.80}$ - $M^{0.85}$ (Figure 5). The log-based *sMR* model exhibited a single sharp peak at $M^{0.75}$, incompatible with the biophysical model of core thermogenesis, which assumes $M^{0.75}$ scaling for whole body *sMR* [8]. Importantly, the *cMR* and *sMR* models exhibited a critical difference in *VIP* statistics (*Variable Importance of Projection* [38]), representing the degree of interdependence among the variables that is constraining the model (Figure 5A, bottom). Across the range *cMR.55cor* - *cMR.70cor*, the *cMR* model depended on all four organ *cMR*s, while the *sMR* model depended only on three (excluding kidney) or two organ *sMRs* (excluding kidney and heart) (Figure 5A, bottom). When scaled to $M^{0.75}$ or $M^{0.80}$, on the other hand,

the *cMRcor* model depended only on a single variable, *cMR.80lvr*, indicating a central role for liver thermogenesis and a lack of constraint by the other Core organs.

We applied two additional tests of the relevance of the estimated organ *cMR*s, first by comparing the Core *cMR*s obtained after varying the combinations of organ *cMR*s, yielding two models that ranked highest with respect to both R^2 and *VIP* statistics: *cMR.70* for heart, kidney and brain, and either *cMR.80* or *cMR.85* for liver (Figure 5B). In order to distinguish between these two combinations, we evaluated their usefulness in the unsupervised classification of major primate clades [39]. After varying the *cMR*s for the liver between *cMR.75* - *cMR.85*, the original set of *mirFam*-based *cMR*s, including *cMR.80lvr*, yielded the lowest value for the information criterion (*AICc*) (Supplementary Figure S5):

cMR.53*cor = 0.53 • *cMR.70kdn* + 0.69 • *cMR.70hrt* + 0.37 • *cMR.80lvr* + 0.09 • *cMR.70brn

In the context of the evolution of thermoregulation, the coefficient of each organ *cMR* in the optimal model may be interpreted as reflecting its relative impact on the total rate of internal thermogenesis, and therefore the degree to which it has been constrained by natural selection.

The evolution of organ cMR tradeoffs conforms to the Core model of thermoregulation.

Bayesian inference revealed generally opposing directions of evolution between body size and *cMR.80lvr*, both between Catarrhini and Glires, as well as within each clade (Figure 6). Among primates, an accelerated increase in liver *cMR* accompanied the decrease in size of two of the smallest Platyrrhini, one of which (*Callithrix pygmaea*) may be heterothermic [40]. All five of the smaller (< 1.0 kg) Platyrrhini exhibited elevated levels of *cMR.80lvr*, consistent with adaptation to a low energy regime and increased reliance on gluconeogenesis. Among all Glires, those species that underwent the greatest reductions in size exhibited the highest increases in liver *cMR.80*, while the largest species (Lagomorphs) exhibited the lowest liver *cMR*s (Figure 6).

Brain *cMR.70* increased in intensity and its rate of evolution accelerated with the divergence of Haplorhini, and again in the case of humans, in contrast to its relative stasis in Lemuriformes and Glires (Figure 6). Compared to their ancestor, the five smallest Platyrrhines exhibited an accelerated *reduction* in brain *cMR*, a clade-wide tradeoff that mirrored the size-related tradeoff in Glires between brain and liver *cMR*s. The relative levels and evolutionary rates of heart *cMR.70* generally tracked body size, with two notable exceptions: the accelerated rates of heart evolution in the clades of the largest Glires (Lagomorpha) and primates (Catarrhini) (Figure 6). In parallel with *cMR.70brn*, humans exhibited an exceptional increase in the rate of evolution of kidney *cMR.70* (Figure 6).

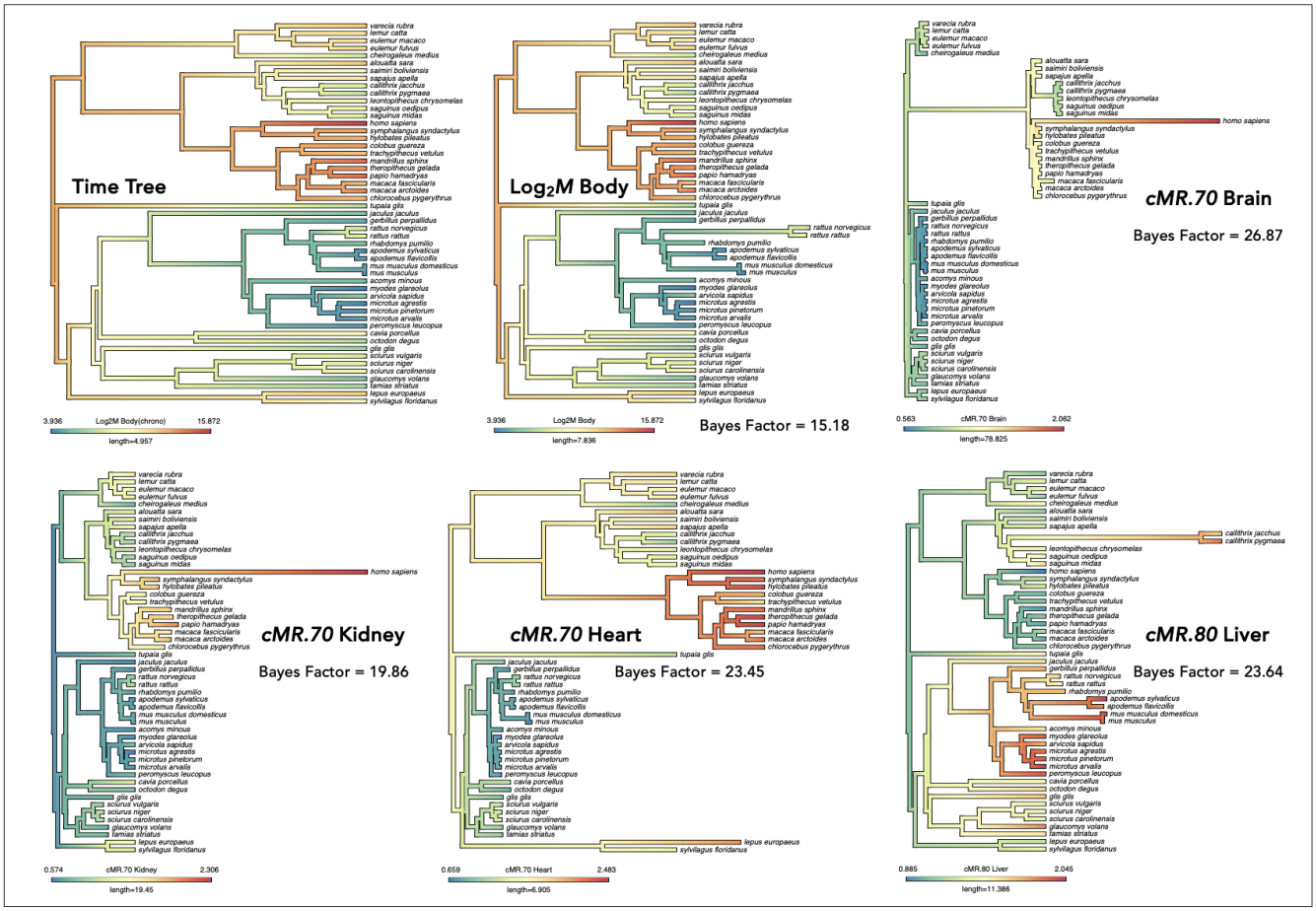

Figure 6. Variable rate phenograms of Log_2M, *cMR.80lvr*, and *cMR.70* of kidney, heart and brain. Bayes factors were computed from the difference between the median log likelihood (*Lh*) of the 1% most likely trees and the median *Lh* of the 1% of trees with the smallest non-zero sum of changes to branch length, *i.e.* those trees most similar to the reference time tree.

DISCUSSION

The recent publication of hundreds of primate genome sequences [41] has been accompanied by ever more fine-grained analysis of the phylogenetic covariance of non-logarithmic traits suspected to have influenced the evolution of brain size [42]: diets richer in calories and protein, larger adipose tissue reserves, and gains in the efficiency or reliability of food acquisition and assimilation, gestation, lactation and infant care [17, 28, 43-48]. For the reasons elaborated above, we submit that an implicit assumption of these studies – that the rate of brain energy expenditure is proportional to log-transformed brain mass – is not justified. The basis of this assumption is that log *rMR* for any related group of species is a linear function of log mass [49]; however, a thermodynamic model composed two terms, proportional to mass and surface area, provides even better estimates of log *rMR* than the conventional power law model [50]. As we have demonstrated, the fixed distribution of organ *sMR*s inferred from the slopes of log *rMRorg*/log *Morg* are unrelated to the distributions of relevant physiological and thermodynamic variables, unlike *mirFam*-based *cMR*s.

Since the seminal analysis by Lande (1979) [29], it has been the convention to base the allometry of brain size on body size [28, 30-31]. Not surprisingly, this approach has not detected anticorrelations among organ sizes [28], given that these are developmentally programmed to track body size [51]. The present study underscores the need to consider the evolution of brain size and energy expenditure in the context of the other principal thermogenic organs. Furthermore, the accelerated evolution of heart *cMR.70* in the largest Glires and primates suggest that cardiovascular adaptations may have been required to ensure adequate rates of blood flow to the brain and heat dissipation.

Comparative studies of the evolution of whole body *rMR* in mammals have consistently yielded log-based allometric exponents ~ 0.75 [49-50]. $M^{0.75}$ was also the optimal allometric scaling we found for a model of stabilizing selection of mammalian *cMRbdy* with respect to *mirFam* [7]. In the present study, log-based organ *sMR* slopes corresponded to the crossover points for the inversion of *cMR* slopes with respect to *mirFam* and organ size, and therefore to the zone of weakest association and constraint by these factors. Thus, adherence of whole body *rMR* to this conserved $M^{0.75}$ allometry appears to allow for variation in organ composition of the Core, such as that imposed by evolutionary enlargement of the brain. This interpretation is further supported by the finding that at $M^{0.75}$, a linear model of *cMRcor* depended on the *cMR* of only a single organ (liver), while the optimal thermoregulatory model (*cMR.53cor*) depended on the *cMR*s of all four thermogenic organs.

Of the six possible *cMR* tradeoffs among four thermogenic organs, why does the brain-liver tradeoff predominate? During the fasting state, once liver glycogen is depleted, the liver is the primary organ of gluconeogenesis: the glucagon-dependent reduction of amino acid or glycerol carbons, fueled by free fatty acids released from adipose tissue. Gluconeogenesis contributes 40 - 60% of total glucose production after an overnight fast, and greater than 90% after 48 hours of fasting [52]. Liver oxidation of fatty acids also generates ketone bodies that provide 60% of the human brain's energy during a prolonged fast, thereby sparing muscle protein [53]. Elevated levels of circulating FA also induce insulin resistance in liver and skeletal muscle, an additional mechanism to ensure an uninterrupted supply of glucose to the brain which, unlike these organs, cannot switch to fatty acid oxidation [53].

The rate of glucose utilization peaks around age five in humans, early in the extended period between weaning and sexual maturity, and the period of slowest growth in body mass[3]. Based on the turnover of isotopically-labeled glucose, glucose production was proportional to brain mass over the entire lifespan, and therefore highest among young children [4]. Among prepubertal children (7 - 9 years of age), the rate of gluconeogenesis was still 50% higher than that found among adolescents [5-6].

The inverse relationship between developmental changes in the brain's glucose uptake and body mass growth rate [3] implicate the liver as the pivotal partner in this ontogenetic tradeoff.

Drawing on metabolite fluxes measured in humans, a computational model of the corresponding fluxes in mice found that following an overnight fast, the rates of liver gluconeogenesis, lipolysis and proteolysis were all elevated ~ 10-fold in mice, relative to the corresponding rates in humans [54]. This comports well with the opposite directions of evolution of *cMR.80lvr* between Glires and primates, which are associated with divergent life history strategies [55-57]. If the evolution of species' liver sizes depended not only on body size, but also on the capacity for glucose production, then improvements in energy reliability might have permitted the observed tradeoffs between liver and other thermogenic organs. Such evolutionary plasticity may have co-opted the liver's inherent mechanism of developmental plasticity: in mammals, only the liver retains full regenerative potential, and Hippo-YAP, the bilaterian regulator of organ size, coordinates liver growth with the suppression of gluconeogenesis [51, 58-61]

Our *cMR*-based model of brain size evolution posits a simple feedback loop between brain size and security of the energy supply: energy security facilitates an increase in brain size which, in turn, facilitates additional improvement in energy reliability, up to the limits imposed by anatomy and physiology, such as the diameter of the birth canal or the limit on the rate of heat dissipation [16]. Fitting *mirFam*, a proxy for the overall rate of energy utilization [7], to the primate brain size dataset of Grabowski et al (2023) [42] using a logistic function, we found that relative brain size was a predictor of *mirFam*, rather than *vice versa*, lending credence to the proposition that evolutionary increases in brain size were, more often than not, associated with greater energy security:

$$\frac{d\,(mirFam)}{d\,(\log M_{brn}/\log M_{bdy})} = r \bullet mirFam\,(1 - mirFam/mirFam_{max}),$$

where r is the growth rate and the range of *mirFam* has been scaled to 1.0.

Given that the relative sizes of the other thermogenic organs can also be fit to logistic models for *mirFam* (Supplementary Figure S6), the question arose as to which relationship might be the principal driver of evolutionary adaptation. In phylogenetic regressions on *mirFam* of organ *cMR*s ranging from *cMR*.60 - *cMR*.80, kidney and heart *cMR*s, and all but one liver *cMR* (*cMR.60lvr*) varied independently of phylogeny (Pagel's *lambd*a = 0), while the variation of brain *cMR*.60 - *cMR*.80 with respect to *mirFam* was secondary to phylogenetic distance (*lambda* = 1 in each case) [34]

, indicating that the divergence of primate clades coincided with changes in the dynamic range of *mirFam* with respect to relative brain size (Supplementary Table S3).

A variable rate phenogram corresponding to this model was generated using the ratios from a Hubbert linearization of the logistic function (Figure 7B) [62]. Thus, the color scale represents the rank on the logistic curve, which generally tracks body size.

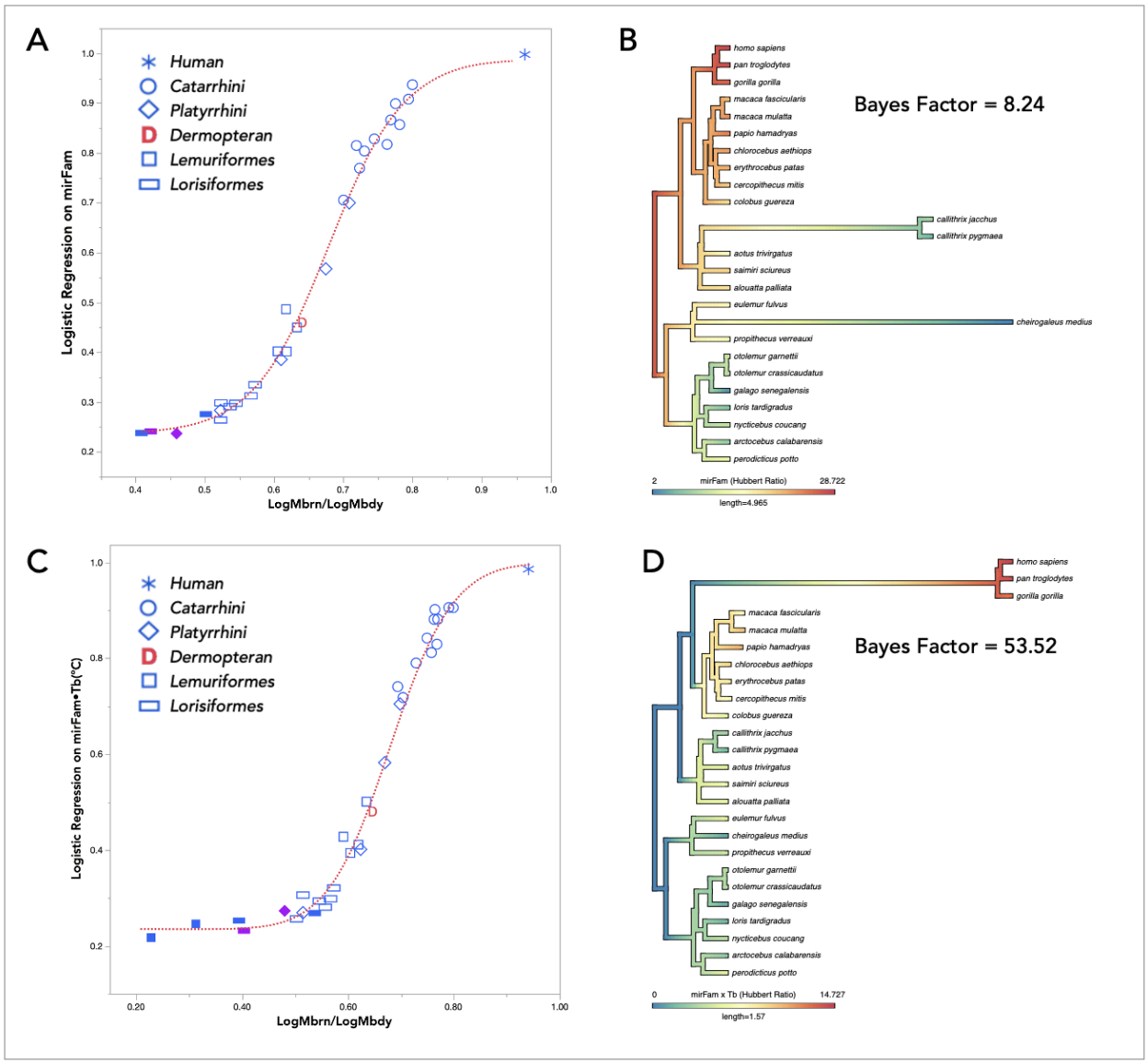

Figure 7. Logistic models of brain size evolution (data from Grabowski et al, 2023) [42]. A, C. For these idealized models (R^2 = 1.00), *mirFam* or *mirFam*•T_b (ºC) was that predicted by the original logistic regression models that excluded the small heterotherm *Cheirogaleus medius*. (original R^2 = 0.88 and 0.85, respectively) (jitter applied). By comparison, logistic regression of Log *Mbdy* on the ratio Log *Mbrn*/Log *Mbdy* yielded R^2 = 0.83. D = *Galeopterus variegatus*. Filled symbols: heterotherms (blue), suspected heterotherms (purple). B, D. Variable rate phenograms of the Hubbert linearization of the corresponding logistic functions.

The three smallest species, a Lemuriform and two species of Callithrix exhibited an accelerated descent in rank: *Cheirogaleus medius* is a heterotherm, and *Callithrix pygmaea* may also be heterothermic [40]. This observation aligns with that previously reported for Callithrichines [31], and suggest that the baseline of the logistic function represents a regime of minimal energy reliability, perhaps related to low calorie-density folivory or insectivory, and consistent with the accelerated rate of evolution of liver *cMR.80* in the *Callithrix* clade.

Following this logic, we postulated that the upper plateau of the logistic model, occupied by primates with the largest relative brain sizes, would correspond to a physiological limit on the rate of heat dissipation [16]. During exercise with progressive hyperthermia, human brain temperature increases in parallel with that of the body core, leading to hyperthermia and fatigue [19-22, 63]. Contemporary chimpanzee populations that find themselves in the hottest and driest savanna landscapes exhibit thermoregulatory behaviors that reduce hyperthermia risk, such as cave use [24]. We previously reported that body temperatures (T_b) in primates are inversely correlated with *mirFam* [7]. Since the highest *mirFam* are found in the largest primates (*Catarrhini*), this trend is reminiscent of the opposite trends, on a broad mammalian scale, between body size [9] and body temperature [10].

Ranking primate species by size revealed conservation of the overall relationship between *mirFam* and body size (Supplementary Figure S7, A), as well as the relationship between *mirFam* and T_b , after correction for phylogeny (Supplementary Figure S7, B). We hypothesized that the product *mirFam* x T_b represents the physiological limit on the rate of heat dissipation limit, given that (a) when ordered according to the rate of Core thermogenesis (*cMR.53cor*), *mirFam* x T_b generally tracked thermal conductance (Supplementary Figure S8, A) and (b) only among Lorisiformes and Lemuriformes, the two earliest-branching clades of primates, did the standardized range of *mirFam* x T_b fall below the range of relative brain size (Supplementary Figure S8, B). In this case, the accelerated evolution detected among hominid apes near the plateau of the *mirFam* x T_b logistic model (Figure 7D) may signal a thermoregulatory adaptation, as it was accompanied by an increase in thermal conductance (Supplementary Figure S8, A).

In keeping with the long-range mammalian trends for body size [9] and body temperature [10], Bayesian inference predicted opposite evolutionary trends for the evolution of the relationship to brain size of *mirFam* and *mirFam* x T_b: descending in rank on the *mirFam* tree, and ascending in rank on the tree for *mirFam x* T_b (Figure 7A and B, respectively). Thus, our logistic model assigns the ancestral primate a high rank with respect to energy reliability and a low rank with respect to the heat

dissipation limit, a propitious combination for the founder of a new order of mammals on a new fitness landscape [64]. In many respects this model, emerging from the reparametrization of rates of energy consumption in terms of *mirFam*-based *cMR*s, fulfills the recent call for an explanation of the distinct pattern of brain size evolution in primates "in terms of the release of a constraint or an adaptive shift that initiated escalating feedback between brain and behavior".[18] Together with the Core model of thermoregulation, it has allowed us to uncover a conserved energy tradeoff that was first proposed 40 years ago in order to account for the expansion of brain size in the human lineage [1]. Since the logistic model is agnostic regarding underlying mechanisms, it may also serve as a null hypothesis for comparison with the evolution of other potentially related adaptations.

The *cMR* approach also has far-reaching implications for evolutionary medicine: for example, the adaptive increase in human kidney *cMR.70* to a level 30% higher than found in other hominoid apes. (By comparison, human kidney *cMR* was 10% *lower* when scaled according to the slope (0.90) of log *rMRkdn*/log *Mkdn*.) Since the kidney is responsible for the homeostasis of pH, nitrogen, sodium, water and glucose, the rapid evolution *cMR.70kdn* in humans may have facilitated adaptations to a diet enriched in lipid and protein [46], and an altered landscape of opportunities for hydration *versus* risks of dehydration ("Savanna hypothesis") [43, 65-67]. A simulation of two million years of African and Eurasian climate and habitats has provided evidence that *H. sapiens* evolved from *H. heidelbergensis* in southern Africa during an unusually warm period that would have necessitated adaptation to hotter, drier conditions [68]. A high density of eccrine sweat glands [26] may have enabled early humans to run down game in long distance pursuits [69], but may also have made them uniquely susceptible to dehydration [27], a marathon-enabling tradeoff. As it is, the kidneys of modern humans are susceptible to damage by heat stress: exposure to 40ºC for as little as one hour is sufficient to redirect blood flow to the skin, reduce blood flow to the kidney by one third [70] and trigger responses promoting water conservation, such as activation of the renin-angiotensin-aldosterone system, that can eventually lead to acute kidney injury [71-72]. Prior to the adaptive increase in *cMR.70kdn*, the kidneys of our hominid ancestors may have been even more vulnerable.

METHODS

Physiological Data

The masses and *rMR*s of the four thermogenic organs were obtained from the dataset of Wang et al (2012) [73], originally derived from the compilation of Navarette et al (2011) [28] (Supplementary Table S1). Values for thermal conductance (C_{min}) were obtained from the dataset of Khaliq et al (2014) [14], substituting congeneric species from the dataset of Wang et al (2012) [73]. Where C_{min} was available for two or more congeneric species, we chose the one with the mass closest to the species in the Wang dataset. Body temperatures were obtained from the AnAge database [74].

MicroRNA Families

Complements of microRNA families were obtained from the most complete assembly for each species using covariance model MirMachine [75], trained on the manually-curated database MirGeneDB2.1 [76] (Supplementary Tables S1 and S2).

Phylogenetic Trees

Using Mesquite © (2021) we derived ultrametric trees for 51 Euarchontoglires or 24 primates from the phylogenies of Alvarez-Carretero et al (2021) [77] and Shao et al (2023) [78], respectively.

Variable Rate Phenograms

Variable rate trees and ancestral node values were inferred using BayesTraits.V4 [79-80] (software available at www.evolution.rdg.ac.uk). Bayes factors for variable rate trees were computed from the difference between the median of the top 1% likelihoods and the median likelihood of the 1% of trees with the smallest non-zero sum of changes to branch length [7]. Phenograms were generated using Phytools [81].

Statistics

Linear, logistic and partial least squares regressions and normal mixture clustering were carried out and visualized using JMP16 ®. All R^2 values were adjusted for the number of predictors. Phylogenetic linear regressions were carried out using the R: CAPER package [82].

DATA AVAILABILITY

The original data with accompanying references are provided in the Supplementary Information Tables S1 and S2.

ACKNOWLEDGMENT

BF is supported by the Tromsø forskningsstiftelse (TFS) [20_SG_BF 'MIRevolution'].

AUTHOR CONTRIBUTIONS

Conceptualization: TS; Methodology: TS; Investigation: BF and TS; Writing – Original Draft: TS; Writing – Review & Editing: BF and TS; Visualization: TS; Funding Acquisition: BF.

DECLARATION OF INTERESTS The authors declare no competing interests.

REFERENCES

1. Armstrong E. 1983. Relative brain size and metabolism in mammals. *Science* 220: 1302-1304.

2. Aiello LC and Wheeler P. 1995. The expensive-tissue hypothesis: the brain and the digestive system in human and primate evolution. *Curr Anthro* 36: 199-221.

3. Kuzawa CW, Chugani HT, Grossman LI, Lipovich L, Muzik O, Hof PR, Wildman DE, Sherwood CC, Leonard WR and Lange N. 2014. Metabolic costs and evolutionary implications of human brain development. *PNAS* 111: 13010-13015.

4. Bier DM, Leake RD, Haymond MW, Arnold KJ, Gruenke LD, Sperling MA and Kipnis DM. 1977. Measurement of "True" Glucose Production Rates in Infancy and Childhood with 6,6-Dideuteroglucose. *Diabetes* 25: 1016-23.

5. Sunehag AL, Treuth MS, Toffolo G, Butte NF, Cobelli C, Bier DM and Haymond MW. 2001. Glucose production, gluconeogenesis, and insulin sensitivity in children and adolescents: an evaluation of their reproducibility. *Ped Res* 50: 115-123.

6. Sunehag AL, Toffolo G. Treuth MS, Butte NF, Cobelli C, Bier DM and Haymond MW. 2002. Effects of dietary macronutrient content on glucose metabolism in children. *J Clin Endocrin Metab*l 87: 5168-5178.

7. Fromm B and Sorger T. 2023. Rapid adaptation of cellular metabolic rate to the microRNA complements of mammals and its relevance to the evolution of endothermy. *iScience*: 108740.

8. Porter WP and Kearney M. 2009. Size, shape, and thermal niche of endotherms. *PNAS* 106: 19666-19672.

9. Baker J, Meade A, Pagel M and Venditti C. 2015. Adaptive evolution toward larger size in mammals. *PNAS* 112: 5093-5098.

10. Avaria-Llautureo J, Hernandez CE, Rodriguez-Serrano E and Venditti, C. 2019. The decoupled nature of basal metabolic rate and body temperature in endotherm evolution. *Nature* 572: 651-654.

11. Naya DE, Spangenberg L, Naya H and Bozinovic F. 2013. Thermal conductance and basal metabolic rate are part of a coordinated system for heat transfer regulation.
Proc Roy Soc B 280: 20131629.

12. Fristoe TS, Burger JR, Balk MA, Khaliq I, Hof C and Brown JH. 2015. Metabolic heat production and thermal conductance are mass-independent adaptations to thermal environment in birds and mammals. *PNAS* 112: 15934-15939.

13. Araújo MB, Ferri-Yáñez F, Bozinovic F, Marquet PA, Valladeres F and Chown SL. 2013. Heat freezes niche evolution. *Ecol Letters* doi: 10.1111/ele.12155 (1-14).

14. Khaliq I, Hof C, Prinzinger R, Böhning-Gaese K and Pfenninger M. 2014.
Global variation in thermal tolerances and vulnerability of endotherms to climate change.
Proc Roy Soc B 281: 20141097.

15. Bennett JM, Sunday J, Calosi P, Villalobos F, Martínez B, Molina-Venegas R, Araújo MB, Algar AC, Clusella-Trulas S, Hawkins BA, Keith SA, Kühn I, Rahbek C, Rodríguez L, Singer A, Morales-Castilla I and Olalla-Tárraga MA. 2021.
The evolution of critical thermal limits of life on Earth. *Nature Comm* 12: 1198 (1-9).

16. Speakman JR and Król E. 2010. Maximal heat dissipation capacity and hyperthermia risk: neglected key factors in the ecology of endotherms. *J Anim Ecol* 79: 726-746.

17. Heldstab SA, Isler K, Graber SM, Schuppli C and van Schaik. 2022.
The economics of brain size evolution in vertebrates. *Curr Biol* 32: R697-R708.

18. Venditti, C, Baker J and Barton RA. 2024. Co-evolutionary dynamics of mammalian brain and body size. *Nat Ecol Evol* https://doi.org/10.1038/s41559-024-02451-3

19. Nybo L. 2012. Brain temperature and exercise performance. *Exp Physiol* 97: 333-339.

20. Wang H, Wang B, Normoyle K, Jackson K, Spitler K, Sharrock MF, Miller CM, Best C, Llano D and Du R. 2014. Brain temperature and its fundamental properties: a review for clinical neuroscientists. *Front Neurosci* 307: 1-17.

21. Sung D, Risk BB, Kottke PA, Allen JW, Nahab F, Fedorov AG and Fleischer CC. 2022.
Comparisons of healthy human brain temperature predicted from biophysical modeling and measured with whole brain MR thermometry. *Nature Sci Rep* 12:19285.

22. Claassen JAHR, Thijssen DHJ, Panerai RB and Faraci FM. 2021. Regulation of cerebral blood flow in humans: physiology and clinical implications of autoregulation. *Physiol Rev* 101: 1487-1559.

23. Pontzer H, Brown MH, Raichlen DA . . . Ross SR. 2016. Metabolic acceleration and the evolution of human brain size and life history. *Nature* 533: 390-393.

24. Lassen NA.1985. Normal average value of cerebral blood flow in younger adults is 50 ml/100 g/min. *J Cereb Blood Flow Metab* 5: 347-349.

25. Lindshield S, Hernandez-Aguilar RA, Korstjens AH . . . Yoshikawa M. 2021. Chimpanzees (*Pan troglodytes*) in savanna landscapes. *Evol Anthropol* 30: 399-420.

26. Kamberova YG, Guhana SM, DeMarchisa A, Jianga J, Wright SS, Morgan BA, Sabetid PC, Tabina CJ, and Lieberman DE. 2018. Comparative evidence for the independent evolution of hair and sweat gland traits in primates. *J Hum Evol* 125: 99–105.

27. Hora M, Pontzer H, Wall-Scheffler CM and Sládek V. 2020. Dehydration and persistence hunting in *Homo erectus*. *J Hum Evol* 138:102682.

28. Navarette A, van Schaik CP and Isler K. 2011. Energetics and the evolution of human brain size. *Nature* 480: 91-93.

29. Lande R. 1979. Quantitative genetic analysis of multivariate evolution, applied to the brain: body size allometry. *Evolution* 33: 402-416.

30. Burger JR, George MA, Leadbetter C and Shaikh F. 2019. The allometry of brain size in mammals. *J Mammal* 100: 276-283.

31. Smaers JB, Rothman RS, Hudson DR, Balanoff AM, Beatty B, Dechmann DKN, deVries D, Dunn, JC, Fleagle JG, Gilbert CC, Goswami A, Iwaniuk AN, Jungers WL, Kerney M, Ksepka DT, Manger PR, Mongle CS, Rohlf FJ, Smith NA, Soligo C, Weisbecker V and Safi K. 2021. The evolution of mammalian brain size. *Sci Adv* 7: eabe2101 (1 - 11).

32. Felsenstein J. 1985. Phylogenies and the comparative method. *Amer Naturalist* 125: 1-15.

33. Hansen TF. 1997. Stabilizing selection and the comparative analysis of adaptation. *Evolution* 51: 1341-1351.

34. Pagel M. 1999. Inferring the historical patterns of biological evolution. *Nature* 401: 877-884.

35. Pagel M, O'Donovan C and Meade A. 2022. General statistical model shows that macro-evolutionary patterns and processes are consistent with Darwinian gradualism. *Nature Comm* 13: 1113.

36. Scholander PF, Hock F, Walters V, Johnson F and Irving L. 1950.
Heat Regulation in Some Arctic and Tropical Mammals and Birds. *Biol Bull* 99: 237-258.

37. de Jong (1993). SIMPLS: An alternative approach to partial least squares regression.
Chemometrics and Intelligent Laboratory Systems 18: 251-263.

38. Wold, S., Johansson, E. and Cocchi, M., 1993. PLS: partial least squares projections to latent structures. In 3D QSAR in *Drug Design: Theory, Methods and Applications*. (pp. 523-550).
Kluwer ESCOM Science Publisher.

39. Celeux G and Govaert G. 1995. Gaussian Parsimonious Clustering Models.
Pattern Recognition 28: 781-793.

40. Tattersall GJ. 2012. Diurnal changes in metabolic rate in pygmy marmosets: Implications for sleep, torpor, and basal metabolism in primates. In: Ruf, T., Bieber, C., Arnold, W., Millesi, E. (eds) *Living in a Seasonal World*, chapter 41: 471-480. Springer.

41. Kuderna LFK, Gao H, Janiak MC . . . Bonet TM. 2023.
A global catalog of whole-genome diversity from 233 primate species. *Science* 380: 9-913.

42. Grabowski M, Kopperud BT, Tsuboi M and Hansen TF. 2023.
Both diet and sociality affect primate brain-size evolution. *Syst Biol* 72: 404-418.

43. Mascia-Lees FE, Relethford JH and Sorger T. 1986.
Perspectives on permanent breast enlargement in human females. *Amer Anthro* 88: 423-428.

44. Martin RD. 1996. Scaling of the mammalian brain: the maternal energy hypothesis.
Physiology 11: 149-156.

45. Isler K and van Schaik CP. 2012. Allomaternal care, life history and brain size evolution in mammals. *J Human Evol* 63: 52-63.

46. Simmen B, Pasquet P, Masi S, Koppert GJA, Wells JCK and Hladik CM. 2017.
Primate energy input and the evolutionary transition to energy-dense diets in humans.
Proc Roy Soc B 284: 20170577.

47. Paine OCC, Koppa A, Henry AG . . . Sponheimer M. 2019. Seasonal and habitat effects on the nutritional properties of savanna vegetation: Potential implications for early hominin dietary ecology. *J Hum Evol* 133: 99-107.

48. Zeller E, Timmermann A, Yun KY, Raia P, Stein K and Ruan J. 2023.
Human adaptation to diverse biomes over the past 3 million years. *Science* 380: 604 - 608.

49. Kleiber M. 1932. Body size and metabolism. *Hilgardia* 6: 315-353.

50. Ballesteros FJ, Martinez VJ, Luque B, Lacasa L, Valor E and Moya A. 2018.
On the thermodynamic origin of metabolic scaling. *Scientific Reports* 8: 1448.

51. Penzo-Méndez AI and Stanger BZ. 2015. Organ-size regulation in mammals.
Cold Spring Harb Perspect Biol 7: a019240.

52. Chung ST, Chacko SK, Sunehag AL and Haymond MW. 2015. Measurements of gluconeogenesis and glycogenolysis: a methodological review. *Diabetes* 64: 3996-4010.

53. Palmer BF and Clegg DJ. 2021. Starvation ketosis and the kidney. *J Nephrol* 52: 467-478.

54. Kummitha CM, Kalhan SC, Saidel GM and Lai N. 2014. Relating tissue/organ energy expenditure to metabolic fluxes in mouse and human: experimental data integrated with mathematical modeling. *Physiol Rep* e12159 (1-20).

55. Jeschke JM, Gabriel W and Kokko H. 2008. r-Strategist/K-Strategists. Jørgensen SE and Fath BD, eds. *Encyclopedia of Ecology*: 3113-3122.

56. Dańko MJ, BurgerO, Argasiński K and Kozłowski J. 2018.
Extrinsic mortality can shape life-history traits, including senescence. *Evol Biol* 45: 395-404.

57. de Vries C, Galipaud M and Kokko H. 2023.
Extrinsic mortality and senescence: a guide for the perplexed. *Peer Community Journal*, 3: e29.

58. Hu Y Shin DJ, Pan H, Lin Z, Dreyfuss JM, Camargo FD, Miao J, and Biddinger SB. 2017.
YAP suppresses gluconeogenic gene expression via PGC1α. *Hepatol* 66: 2029–2041.

59. Cox AG, Tsomides A, Yimlamai D . . . Goessling W. 2018. Yap regulates glucose utilization and sustains nucleotide synthesis to enable organ growth. *EMBO J* 37: e100294.

60. Ibar C and Irvine KD. 2020. Integration of Hippo-Yap signaling with metabolism.
Dev Cell 54: 256-267.

61. Driskill JH and Pan D. 2021. The Hippo pathway in liver homeostasis and pathophysiology.
Ann Rev Pathol Mech Dis 16: 299-322.

62. Hubbert MK. 1982. Techniques of prediction as applied to the production of oil and gas.
In Gass, Saul I. (ed.) *Oil and Gas Supply Modeling* (proceedings of a symposium held at the Department of Commerce, Washington, DC, June 18–20, 1980). NBS Special Publication 631. Washington (DC): National Bureau of Standards. pp. 16–141.

63. Tsuji B, Hayashi K, Kondo N and Nishiyasu T. 2016.
Characteristics of hyperthermia-induced hyperventilation in humans. *Temperature* 3: 146-160.

64. Duran-Nebreda S, Bentley RA, Vidiella B, Spiridonov A, Eldredge N, O'Brien MJ and Valverde S. 2024. On the multiscale dynamics of punctuated evolution.
Trends Ecol Evol: doi.org/10.1016/j.tree.2024.05.003 (1 - 11).

65. Dart, RA. 1925. Australopithecus africanus: the man–ape of South Africa. *Nature* 115: 195-199.

66. Reed KE. 1997. Early hominid evolution and ecological change through the African Plio-Pleistocene. *J Hum Evol* 32: 289-322.

67. Davies TJ, Daru BH, Bezeng BS . . . Bond WJ. 2020. Savanna tree evolutionary ages inform the reconstruction of the paleoenvironment of our hominin ancestors. *Sci Rep* 10: 12430.
68. Timmermann A, Yun KS, Raia P . . . Ganopolski. 2022. Climate effects on archaic human habitats and species succession. *Nature* 604: 495-501.

69. Morin E and Winterhalder B. 2024. Ethnography and ethnohistory support the efficiency of hunting through endurance running in humans. *Nature Hum Behav* 8: 1065–1075.

70. Rowell LB. 1974. Human cardiovascular adjustments exercise and thermal stress.
Physiol Rev 54: 75-159.

71. Chapman CL, Johnson BD, Vargas NT, Hostler D, Parker MD, Schlader ZJ. Both hyperthermia and dehydration during physical work in the heat contribute to the risk of acute kidney injury.
J Appl Physiol 128: 715–728.

72. Chapman CL, Johnson BD, Parker MD, Hostler D, Pryor RR and Schlader Z. 2021.
Kidney physiology and pathophysiology during heat stress and the modification by exercise dehydration, heat acclimation and aging. *Temperature* 8: 108-159.

73. Wang ZM, Zhang J, Ying Z and Heymsfield SB. 2012. Organ-tissue level model of resting energy expenditure across mammals: new insights into Kleiber's Law. *ISRN Zool*: 673050.

74. Magalhães JP, Abidi Z, dos Santos GA . . . Ka Po To P. 2024. Human Ageing Genomic Resources: updates on key databases in ageing research. *Nucl Acids Res* 52: D900-D908.

75. Umu SU, Paynter VM, Trondsøn H, Buschmann T, Rounge TB, Peterson KJ and Fromm B. 2023. Accurate microRNA annotation of animal genomes using trained covariance models of curated microRNA complements in MirMachine. *Cell Genomics* 3: 100348.

76. Fromm B, Høye E, Domanska D, Zhong X, Aparicio-Puerta E, Ovchinnikov V, Umu SU, Chabot, PJ, Kang W, Aslanzadeh M, Tarbier M, Mármol-Sánchez E, Urgese G, Johansen M, Hovig E, Hackenberg M, Friedländer MR and Peterson KJ. 2021. MirGeneDB 2.1: toward a complete sampling of all major animal phyla. *Nucl Acids Res* 50: D204-D210.

77. Álvarez-Carretero S, Tamuri A, Battini M, Nascimento F, Carlisle E, Asher R, Yang Z, Donoghue P and Dos Reis M. 2022. A species-level timeline of mammal evolution integrating phylogenomic data. *Nature* 602: 263-267.

78. Shao Y, Zhou, Li F . . . Wu DD. 2023.
Phylogenomic analyses provide insights into primate evolution. *Science* 380: 913-924.

79. Pagel M, Meade A and Barker D. 2004.
Bayesian estimation of ancestral character states on phylogenies. *Syst Biol* 53: 673-684.

80. Venditti C, Meade A. and Pagel M. 2011.
Multiple routes to mammalian diversity. *Nature*, 479, 393-396.

81. Revell LJ. 2012. phytools: an R package for phylogenetic comparative biology (and other things). *Methods Ecol Evol* 3: 217-223.

82. Orme D, Freckleton RP, Thomas GH and Petzoldt T. 2013. CAPER: comparative analyses of phylogenetics and evolution in R. *Methods Ecol and Evol* 3: 141-151.

SUPPLEMENTARY INFORMATION

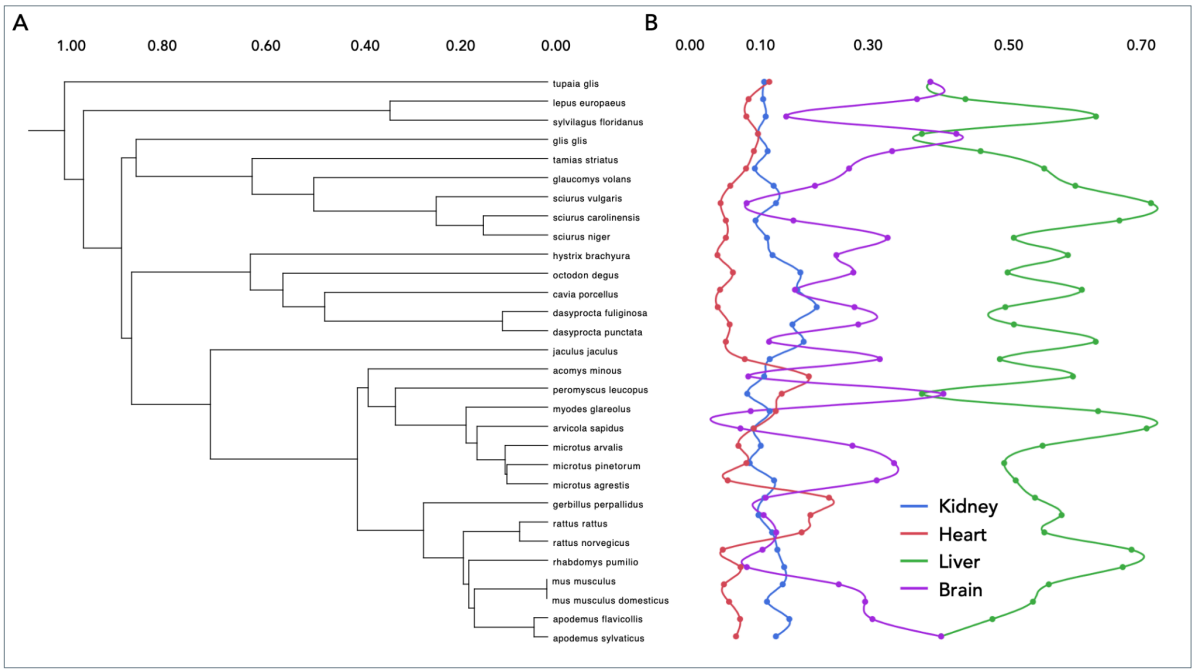

Figure S1. The proportions of brain and liver vary reciprocally in the Euarchontoglires Core. Species include one Scandentia, two Lagomorpha, and 27 Glires, including three Sciuridae.
A. Ultrametric phylogenetic tree. The scale bar represents relative time of divergence.
B. Mass proportion of each organ relative to the total Core mass.

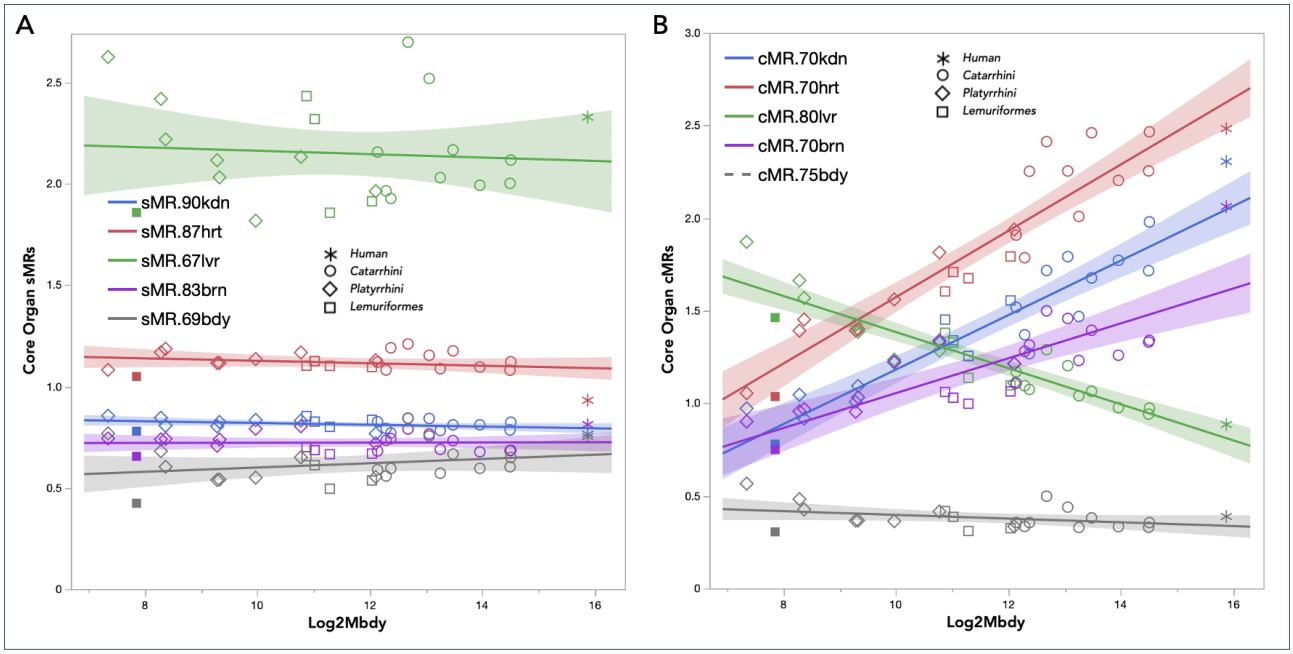

Figure S2. *cMR* slopes vary with size, while an *sMR* slope is independent of size.
A. Log-based *sMR* slopes are independent of organ or body size ($N = 24$).
B. Estimated *cMR* slopes for four thermogenic organs compared to the Kleiber whole-body *sMR*. See the legend to Figure 3 for details on the estimation of organ *cMR*s.

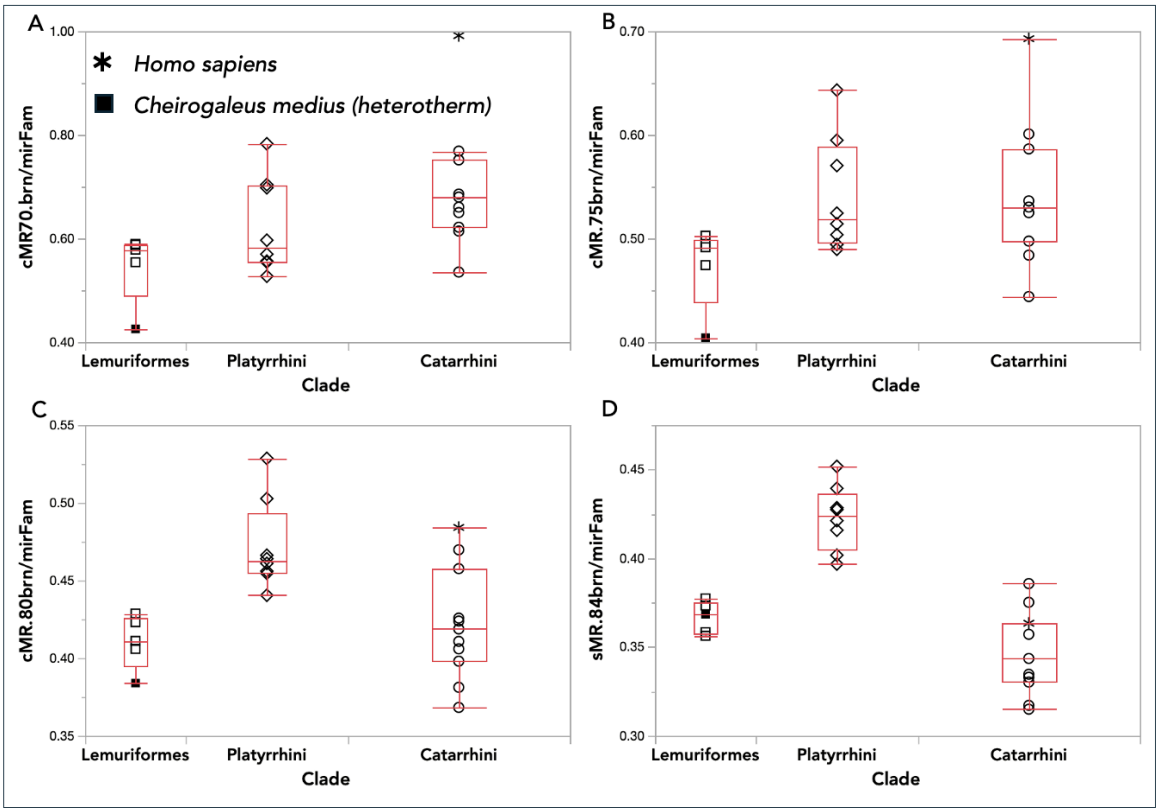

Figure S3. Comparison of the distribution among 24 primates of the ratios with respect to *mirFam* of *cMR.70brn*, *cMR.75brn* and *cMR.80brn* (A - C), and the ratio to *mirFam* of log-based *sMR.84* (D) (log *rMRbrn*/log *Mbrn* = 0.84, $sMRbrn = rMRbrn/M^{0.84}$).

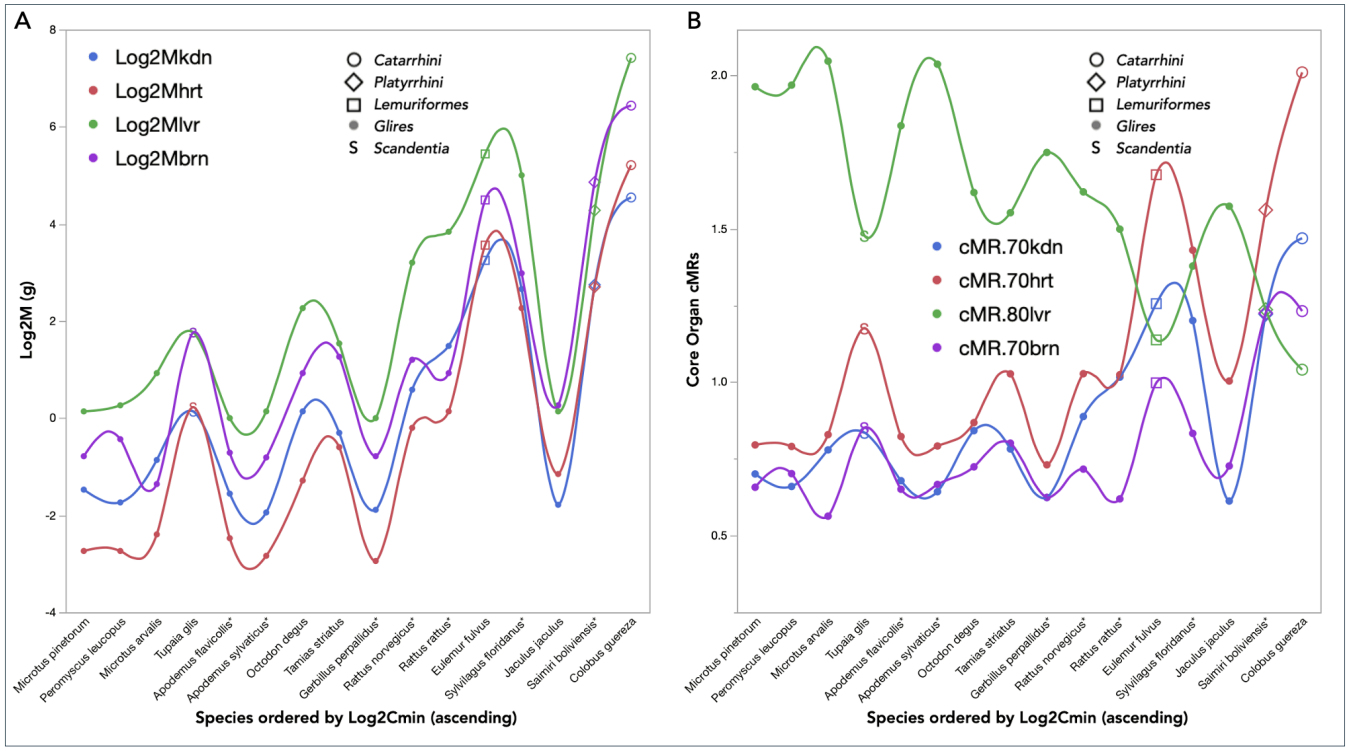

Figure S4. Thermal conductance also covaries with *cMR* tradeoffs between liver and brain.
A. Thermal conductance is a direct function of whole body size, and therefore of organ size.
B. The size-related increase in thermal conductance is related to a compensatory tradeoff in core thermogenesis between liver, on the one hand, and kidney, heart and brain, on the other.
Asterisks (*) represent species in the 4-organ dataset of Wang et al (2012) [65] that have been substituted for congeneric species in the C_{min} dataset of Khaliq et al (2014) [14].

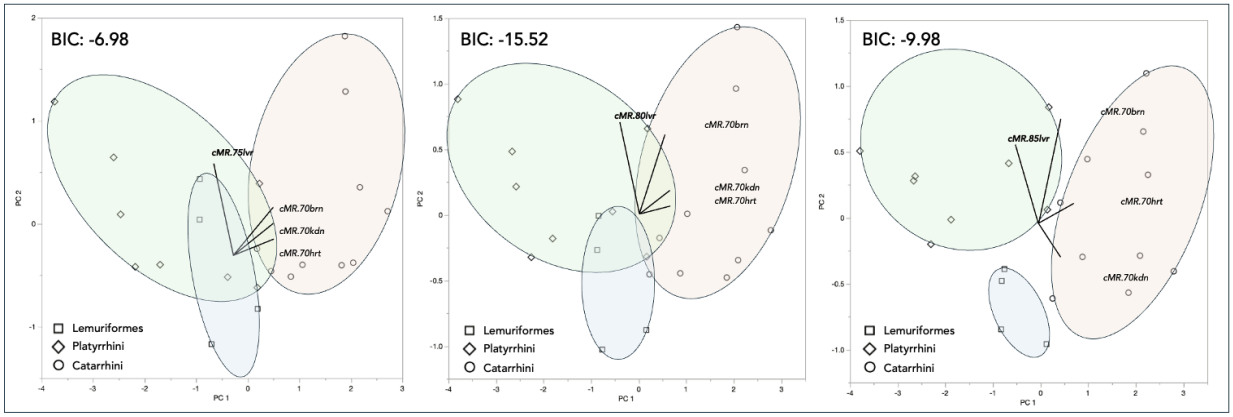

Figure S5. Unsupervised classification of primate clades based on Core *cMR* composition.
Principal components were calculated from each *cMR* correlation matrix, and membership in two clusters estimated by expectation maximization of their joint probability distributions.
Kidney, heart and brain *cMR* = *cMR.70*; liver *cMR*s were varied between *cMR.75lvr* - *cMR.85lvr* (bold type). Ellipses were hand-drawn to include all members of the three phylogenetic clades.

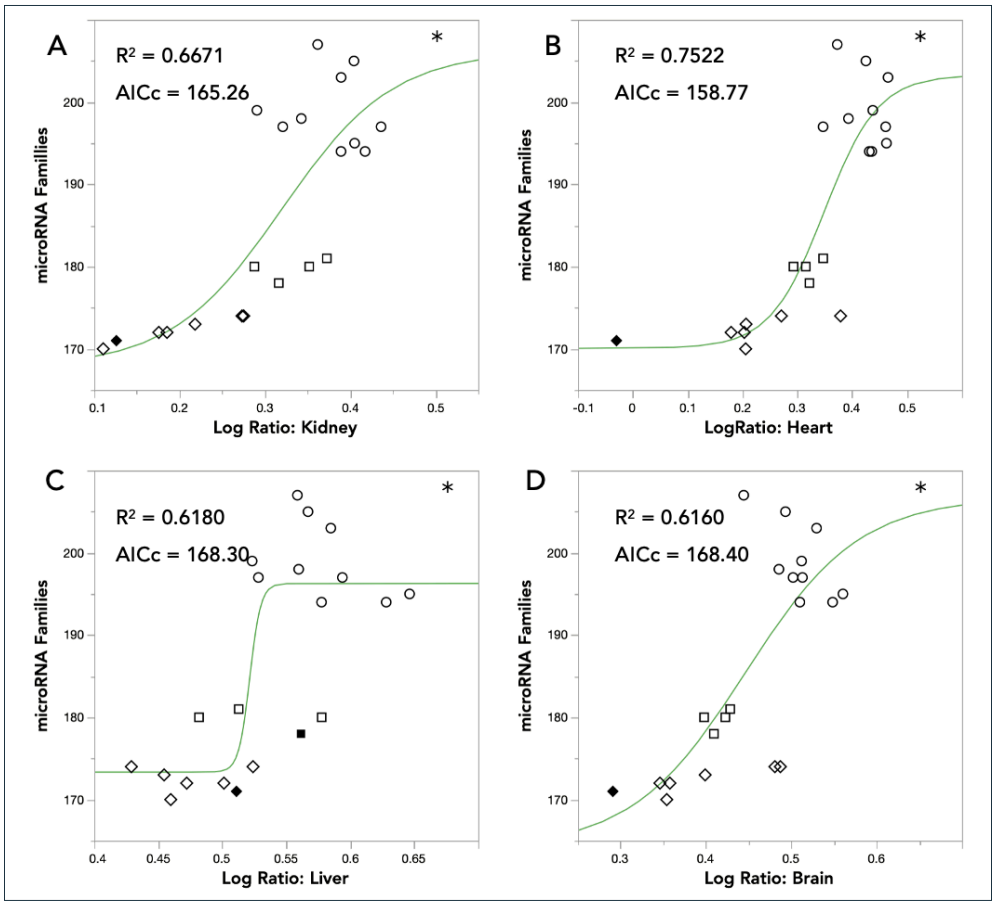

Figure S6. Logistic models for evolution of the relative size of four thermogenic organs. Symbols representing clades as in previous figures, with filled symbols representing heterotherms.

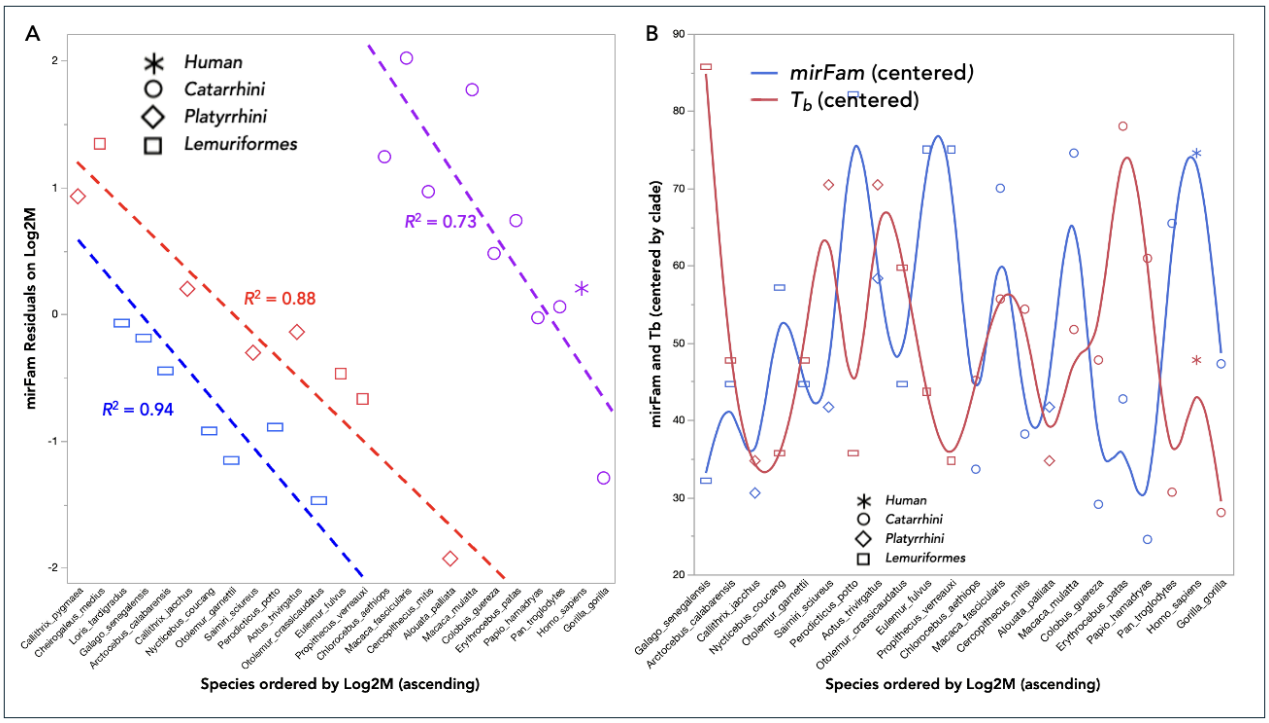

Figure S7. Conservation of *mirFam* and *mirFam* x T_b.
A. The *mirFam*-$\log_2 M$ relationship is least conserved among Catarrhini (purple).
B. Visualization of the reciprocal variation of *mirFam* and T_b. In order to control for phylogeny, the data were range-standardized for Catarrhini, Lorisiformes, and Platyrrhini+Lemuriformes.

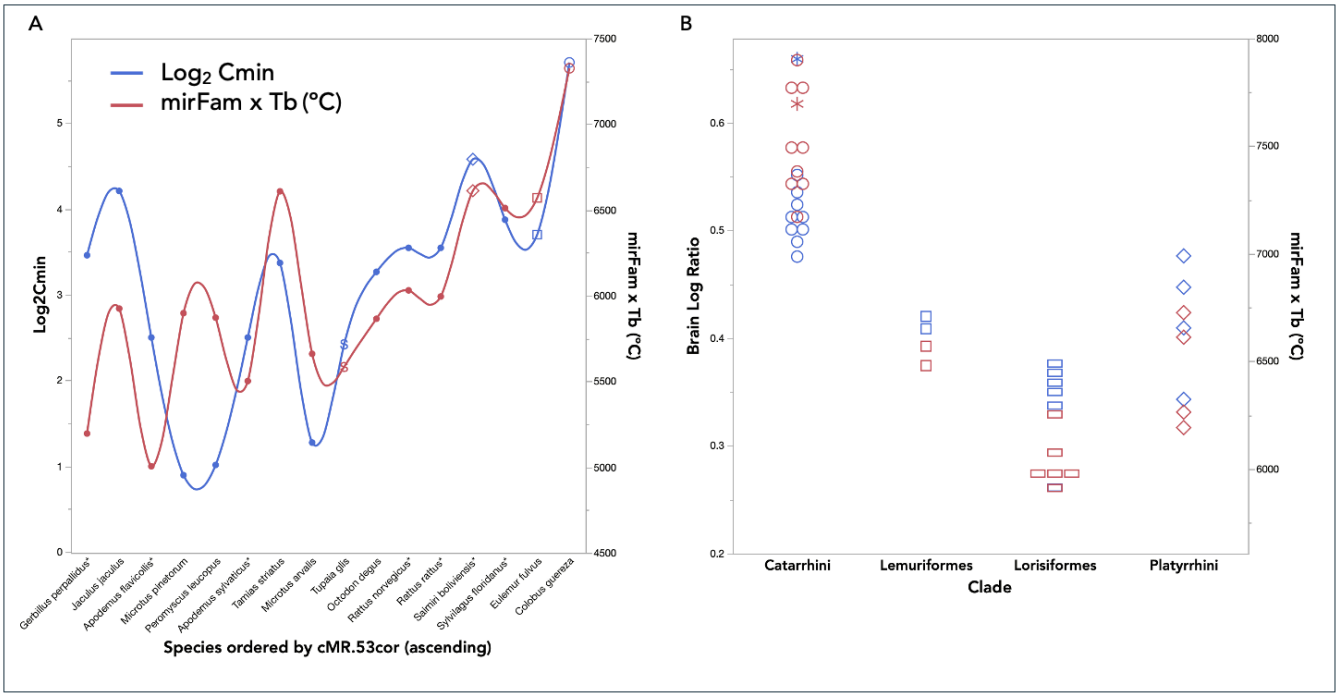

Figure S8. *mirFam* x T_b behaves as a proxy for the physiological limit on heat dissipation.
A. *mirFam* x T_b generally tracks thermal conductance in Euarchontoglires.
B. The range of *mirFam* x T_b falls below the range of relative brain size only in the earliest-branching clades of primates (Strepsirrhini).

Table S1. Summary of species *mirFam*, mass and resting *MR*s for organs, Core and body. All physiological data were obtained from Wang et al (2012) [65], most of which were compiled by Navarette et al (2011) [28]. The names of the indicated taxa were substituted with congeneric species on the phylogenies of Álvarez-Carretero et al (2022) [69] and Shao et al (2023) [70].

Clade	Wang Taxon Names	Names on Phylogeny	*mirFam*	*Mkdn* (g)	*Mhrt* (g)	*Mlvr* (g)	*Mbrn* (g)	*Mcor* (g)	*Mbdy* (g)	*MRkdn* (W)	*MRhrt* (W)	*MRlvr* (W)	*MRbrn* (W)	*MRcor* (W)	*MRbdy* (W)
Primates	*Alouatta sara*	*Alouatta palliata*	174	9.9	24	81.2	56.5	171.6	4399.6	13.7088	13.6112	33.6452	12.9948	73.96	169.5872
Primates		*Callithrix jacchus*	172	2.9	2.8	17.8	7.3	30.8	311.8	6.039	17.928	37.352	20.453	81.772	180.7072
Primates	*Cebualla pygmaea*	*Callithrix pygmaea*	171	1.9	0.86	13.5	4.4	20.66	162.66	6.8432	11.1622	29.0377	20.9296	67.9727	112.3625
Primates		*Cheirogaleus medius*	176	1	0.93	6.3	2.8	11.03	231.03	1.5238	0.94858	15.012	2.5432	20.02758	25.77858
Primates		*Chlorocebus pygerythrus*	199	12.1	42.6	89	80.8	224.5	5300.5	2.204	2.8616	16.643	3.8471	25.5557	35.7841
Primates		*Colobus guereza*	198	23.3	37	171	86.5	317.8	9749.8	2.9356	3.5644	14.553	6.2832	27.3362	46.7808
Primates		*Eulemur fulvus*	180	9.5	11.8	43.4	22.5	87.2	2500.2	1.4364	3.3495	13.248	4.0794	22.1133	33.0213
Primates		*Eulemur macaco*	180	14.2	9.1	77.8	24.2	125.3	1875.3	2.2227	3.4817	16.2184	4.78	26.7028	45.6892
Primates	Human	*Homo sapiens*	208	250	320	1700	1300	3570	59970	9.2862	14.1312	40.05	25.56	89.0274	199.0161
Primates	*Hylobates concolor*	*Hylobates pileatus*	195	35.2	58.2	293	137.8	524.2	6550.2	13.3043	25.16	63.612	27.9395	130.0158	323.3718
Primates		*Lemur catta*	178	11.2	11.7	72.9	22.8	118.6	2074.6	12.789	17.135	50.27	15.162	95.356	195.6392
Primates		*Leontopithecus chrysomelas*	173	4.1	3.8	18.9	13.2	40	642	27.4	39.162	78.566	35.518	180.646	471.706
Primates	*Macaca nigra*	*Macaca arctoides*	205	50	61	241	118	470	15870	42.6393	63.242	115.64	49.59	271.1113	669.3613
Primates	Monkey	*Macaca fascicularis*	207	21	23	110	42	196	4500	21.394	51.5696	84.252	44.5244	201.74	419.94
Primates		*Mandrillus sphinx*	194	49.9	76	331	168	624.9	23024.9	0.8932	1.31274	3.9304	2.006	8.14234	13.62034
Primates		*Papio hamadryas*	197	80.3	103	392	174	749.3	23249.3	2.229	2.4725	9.2769	3.8025	17.7809	31.2792
Primates	*Saguinus lagonotus*	*Saguinus midas*	170	1.9	3.3	14.4	7.8	27.4	330.4	0.2841	0.2094	2.2764	0.56832	3.33822	4.47022
Primates		*Saguinus oedipus*	172	3.1	3.7	20.9	10	37.7	623.7	0.23424	0.1456	1.39829	0.2828	2.06093	2.90093
Primates		*Saimiri boliviensis*	174	6.7	6.5	19.4	29	61.6	1002.6	0.609	0.34636	3.7466	0.7304	5.43236	8.15126
Primates		*Sapajus apella*	171	10.4	13.4	49.3	50.8	123.9	1749.9	0.5126	0.25916	3.4181	0.29133	4.48119	5.79399
Primates		*Symphalangus syndactylus*	194	43.7	51.5	294	143	532.2	8500.2	1.179	0.93177	9.5588	1.2834	12.95297	20.57737
Primates		*Theropithecus gelada*	203	38	77.2	236	140.9	492.1	11402.1	0.27412	0.10241	1.43344	0.29232	2.10229	2.94789
Primates		*Trachypithecus vetulus*	197	15.4	19.2	90	72	196.6	4999.6	0.47379	0.21728	3.2058	0.3715	4.26837	5.62837
Primates		*Varecia rubra*	181	22.4	18.1	72.2	35.7	148.4	4200.4	0.25038	0.19992	2.1967	0.44973	3.09673	4.03113
Scandentia		*Tupaia glis*	151	1.1	1.17	3.4	3.4	9.07	141.07	0.31892	0.24768	1.835	0.46055	2.86215	4.13635
Glires		*Acomys minous*	157	0.32	0.18	0.9	0.9	2.3	42.3	0.779	0.98487	6.3756	1.54	9.67947	18.10547
Glires		*Apodemus flavicollis*	141	0.34	0.18	1	0.61	2.13	25.13	7.2688	9.5589	41.0427	9.1884	67.0588	118.8928
Glires		*Apodemus sylvaticus*	155	0.26	0.14	1.1	0.57	2.07	18.07	6.0705	9.4282	23.219	8.82	47.5377	109.5518
Glires		*Arvicola sapidus*	149	0.7	0.28	2.6	1.1	4.68	61.68	9.301	7.5257	44.9684	9.8736	71.6687	118.9187
Glires	Guinea Pig	*Cavia porcellus*	174	5.6	2.3	27	4.7	39.6	799.6	4.623	5.785	13.2502	12.934	36.5922	64.7281
Glires		*Gerbillus perpallidus*	147	0.27	0.13	1	0.58	1.98	29.98	110	140.8	340	312	902.8	1489.36
Glires		*Glaucomys volans*	176	0.59	0.56	2.9	1.9	5.95	54.95	20.768	41.4966	121.302	47.1276	230.6942	362.6636
Glires		*Glis glis*	168	0.68	0.48	3.2	1.5	5.86	83.86	25.2149	35.5865	113.484	47.047	221.3324	388.6604
Glires		*Jaculus jaculus*	158	0.29	0.45	1.1	1.2	3.04	48.04	7.26	31.1406	38.982	28.4416	105.8242	221.0494
Glires		*Lepus europaeus*	173	18.5	28.9	90.4	14.8	152.6	3338.6	26.4969	46.74	97.645	48.048	218.9299	617.6499
Glires		*Microtus agrestis*	148	0.17	0.12	0.63	0.39	1.31	15.31	11.544	22.3108	44.748	5.5648	84.1676	162.2246
Glires		*Microtus arvalis*	153	0.55	0.19	1.9	0.39	3.03	27.03	4.3533	4.2864	22.048	3.5392	34.2269	61.949
Glires		*Microtus pinetorum*	154	0.36	0.15	1.1	0.58	2.19	21.19	0.57664	0.57312	4.256	0.954	6.35976	9.89316
Glires		*Mus musculus*	167	0.28	0.07	0.68	0.36	1.39	15.39	0.67473	0.76758	3.6366	1.4784	6.55731	10.79621
Glires	Mouse	*Mus musculus domesticus*	167	0.51	0.16	1.8	0.5	2.97	27.97	0.51802	0.70224	4.3094	1.2825	6.81216	9.19356
Glires		*Myodes glareolus*	143	0.24	0.1	0.67	0.35	1.36	15.36	1.3056	1.7629	5.3185	3.3831	11.7701	21.4049
Glires		*Octodon degus*	156	1.1	0.41	4.8	1.9	8.21	129.21	2.304	2.6488	12.8904	3.6075	21.4507	39.9589
Glires		*Peromyscus leucopus*	160	0.3	0.15	1.2	0.74	2.39	22.39	0.8998	0.46494	5.6736	1.1343	8.17264	13.26674
Glires		*Rattus norvegicus*	168	1.5	0.87	9.2	2.3	13.87	209.87	3.9368	2.1022	19.602	2.1667	27.8077	51.4437
Glires	Rat	*Rattus rattus*	167	2.8	1.1	14.3	1.9	20.1	390.1	0.25752	0.57375	1.6973	0.8256	3.35417	5.59067
Glires		*Rhabdomys pumilio*	161	0.41	0.21	1.8	0.6	3.02	50.02	0.28704	0.23274	1.4337	0.63	2.58348	4.61148
Glires		*Sciurus carolinensis*	175	3.2	2.8	16.4	7.5	29.9	595.9	0.34272	0.21075	2.1175	0.44892	3.11989	4.20479
Glires		*Sciurus niger*	165	3	2.5	10.7	7.5	23.7	412.7	0.16592	0.17472	1.31481	0.31512	1.97057	2.81057
Glires		*Sciurus vulgaris*	175	1.7	1.7	5.5	6.3	15.2	274.2	0.24948	0.17511	1.748	0.4263	2.59889	4.10249
Glires		*Sylvilagus floridanus*	170	6.3	4.8	32	7.9	51	972	2.0888	1.0945	12.584	0.9709	16.7382	29.7252
Glires		*Tamias striatus*	173	0.81	0.66	2.9	2.4	6.77	103.77	0.36285	0.26607	2.7414	0.4098	3.78012	6.09722

Table S2. Primate microRNA families, brain volume (ECV), body mass and temperature. Endocranial volume (ECV) and body mass were obtained from Grabowski et al (2023) [42]. Body temperatures were retrieved from the AnAge database (Magalhães et al, 2024) [67].

Order	Species	*mirFam*	ECV	Mass (g)	T_b (°C)
Catarrhini	*Homo sapiens*	208	1252.00	50000	37.0
Catarrhini	*Pan troglodytes*	206	368.35	44967	35.7
Catarrhini	*Gorilla gorilla*	202	490.41	120950	35.5
Catarrhini	*Macaca fascicularis*	207	63.98	4251	37.6
Catarrhini	*Macaca mulatta*	208	88.98	6793	37.3
Catarrhini	*Papio hamadryas*	197	146.17	14150	38.0
Catarrhini	*Chlorocebus aethiops*	199	65.00	3720	36.8
Catarrhini	*Erythrocebus patas*	201	97.73	9450	39.3
Catarrhini	*Cercopithecus mitis*	200	71.33	6109	37.5
Catarrhini	*Colobus guereza*	198	74.39	8589	37.0
Platyrrhini	*Callithrix jacchus*	172	7.24	320	36.0
Platyrrhini	*Callithrix pygmaea*	171	4.17	116	35.2
Platyrrhini	*Aotus trivirgatus*	177	16.85	989	38.0
Platyrrhini	*Saimiri sciureus*	174	24.14	799	38.0
Platyrrhini	*Alouata palliata*	174	49.88	6250	36.0
Lemuriformes	*Eulemur fulvus*	180	25.77	2292	36.5
Lemuriformes	*Cheirogaleus medius*	176	2.60	140	38.0
Lemuriformes	*Propithecus verreauxi*	180	26.21	2955	36.0
Lorisiformes	*Otolemur garnettii*	166	11.50	764	36.0
Lorisiformes	*Otolemur crassicaudatus*	166	11.78	1150	36.6
Lorisiformes	*Galago senegalensis*	165	3.96	194	37.9
Lorisiformes	*Loris tardigradus*	166	5.87	193	35.5
Lorisiformes	*Nycticebus coucang*	167	10.13	653	35.4
Lorisiformes	*Arctocebus calabarensis*	166	6.92	309	36.0
Lorisiformes	*Perodicticus potto*	169	12.42	835	35.4

Supplementary Table S3. Phylogenetic regressions of primate organ *cMR*s on *mirFam*. For reference, see the logistic regressions of *mirFam* on relative organ size (Supplementary Figure S6).

	Allometric Exponent	Pagel's *lambda*	R^2	*P*	*AICc*
KIDNEY	0.80	0	0.5366	6.39E-05	-42.7
	0.75	0	0.5834	2.14E-05	-20.09
	0.70	0	0.5958	1.56E-05	-0.93
	0.65	0	0.5946	1.61E-05	16.22
	0.60	0	0.5859	2.00E-05	32.13
		Pagel's *lambda*	R^2	*P*	*AICc*
HEART	0.80	0	0.4937	1.60E-04	-38.02
	0.75	0	0.6476	3.83E-06	-17.88
	0.70	0	0.6962	8.44E-07	0.63
	0.65	0	0.7133	4.69E-07	17.65
	0.60	0	0.7163	4.21E-07	33.66
		Pagel's *lambda*	R^2	*P*	*AICc*
LIVER	0.80	0	0.5724	2.79E-05	-15.22
	0.75	0	0.4011	9.28E-04	-10.98
	0.70	0	0.0854	1.01E-01	-2.86
	0.65	0	-0.0344	5.89E-01	10.24
	0.60	0.962	0.0145	2.66E-01	27.34
		Pagel's *lambda*	R^2	*P*	*AICc*
BRAIN	0.80	1	0.0329	2.05E-01	-63.9
	0.75	1	0.107	7.55E-02	-35.75
	0.70	1	0.1336	5.07E-02	-10.58
	0.65	1	0.151	4.17E-02	11.76
	0.60	1	0.1596	3.71E-02	32.24